

INSTRUCTLAYOUT: Instruction-Driven 2D and 3D Layout Synthesis with Semantic Graph Prior

Chenguo Lin*, Yuchen Lin*, Panwang Pan, Xuanyang Zhang, and Yadong Mu

Abstract—Comprehending natural language instructions is a charming property for both 2D and 3D layout synthesis systems. Existing methods implicitly model object joint distributions and express object relations, hindering generation’s controllability. We introduce INSTRUCTLAYOUT, a novel generative framework that integrates a semantic graph prior and a layout decoder to improve controllability and fidelity for 2D and 3D layout synthesis. The proposed semantic graph prior learns layout appearances and object distributions simultaneously, demonstrating versatility across various downstream tasks in a zero-shot manner. To facilitate the benchmarking for text-driven 2D and 3D scene synthesis, we respectively curate two high-quality datasets of layout-instruction pairs from public Internet resources with large language and multimodal models. Extensive experimental results reveal that the proposed method outperforms existing state-of-the-art approaches by a large margin in both 2D and 3D layout synthesis tasks. Thorough ablation studies confirm the efficacy of crucial design components.

Index Terms—layout synthesis, controllable generation, graph diffusion models, scene graphs.



1 INTRODUCTION

AUTOMATICALLY synthesizing controllable and appealing 2D and 3D layouts has been a challenging task for computer vision and graphics [1; 2; 3; 4; 5; 6; 7; 8; 9; 10; 11; 12; 13; 14; 15], which requires building a generative model by multimodal conditional information. An ideal layout synthesis system should fulfill at least three objectives: (1) comprehending instructions in natural languages, thus providing an intuitive and user-friendly interface; (2) designing object compositions that exhibit aesthetic appeal and thematic harmony; (3) placing objects in appropriate positions adhering to their functions and regular arrangements.

To enhance the controllability of layout synthesis, we need to address natural language instructions as inputs. However, natural instructions for layout design often rely on abstract object relationships, which has posed a significant challenge for recent advancements in 2D and 3D layout synthesis. Previous works [16; 17; 18; 19; 20; 21] primarily exclude instructional prompts or do not prioritize them, leading to a low level of controllability and interpretability in the generated layouts. Other studies [22; 23; 24] utilize relation graphs to provide explicit control over object interactions, which are, however, too complicated and fussy for human users to specify. Moreover, previous works merely represent objects by categories [6; 17; 19; 22] or low-dimensional features [11; 12; 21; 25] which lack visual appearance details, resulting in style inconsistency and constraining customization options in layout synthesis.

To address these issues, we present INSTRUCTLAYOUT, a novel generative framework for both 2D and 3D layout

synthesis with natural language instructions. Figure 1 illustrates the overview of proposed method. INSTRUCTLAYOUT basically comprises two parts: a **semantic graph prior** and a **layout decoder**. In the first stage, it takes instructions about partial object arrangement and attributes as conditions and learns the conditional distribution of semantic graphs for the holistic layout. In the second stage, harnessing the well-structured and informative graph latents, the layout decoder can easily generate 2D poster and 3D scene layouts that exhibit semantic consistency while closely adhering to the provided instructions. For 2D poster layout synthesis, we additionally provide a **tagline generator** to fill the bounding boxes with text content for real-world applications. With the learned semantic graph prior, INSTRUCTLAYOUT also achieves a wide range of instruction-driven generative tasks in a zero-shot manner.

Specific conditional diffusion models are devised for both parts of INSTRUCTLAYOUT. Benefitting from the two-stage scheme, it can separately handle discrete and continuous attributes of layouts, drastically reducing the burden of network optimization. To enhance the capability of aesthetic design, INSTRUCTLAYOUT utilizes the naturally discrete features of 2D objects, such as fonts, colors, and shapes. In contrast, in terms of 3D objects, it leverages object geometrics and appearances by quantizing semantic features from a multimodal-aligned model [26]. Consequently, our model can handle these discrete features in a unified manner.

To fit practical scenarios and promote the benchmarking of instruction-drive layout synthesis, we curate **two high-quality datasets** containing paired layouts and instructions with the help of large language and multimodal models [27; 28; 29] for both 2D E-commerce poster and 3D indoor scene synthesis tasks. Comprehensive quantitative evaluations reveal that INSTRUCTLAYOUT surpasses previous state-of-the-art methods by a large margin in terms of both generation controllability and fidelity. Each essential component of our method is carefully verified through

• *: equal contribution. C. Lin, Y. Lin and Y. Mu are with Wangxuan Institute of Computer Technology, Peking University. P. Pan and X. Zhang are with PICO AI group, ByteDance.
E-mail: {chenguolin, linyuchen}@stu.pku.edu.cn, {panpanwang, zhangxuanyang}@bytedance.com, myd@pku.edu.cn.
Corresponding author: Yadong Mu.

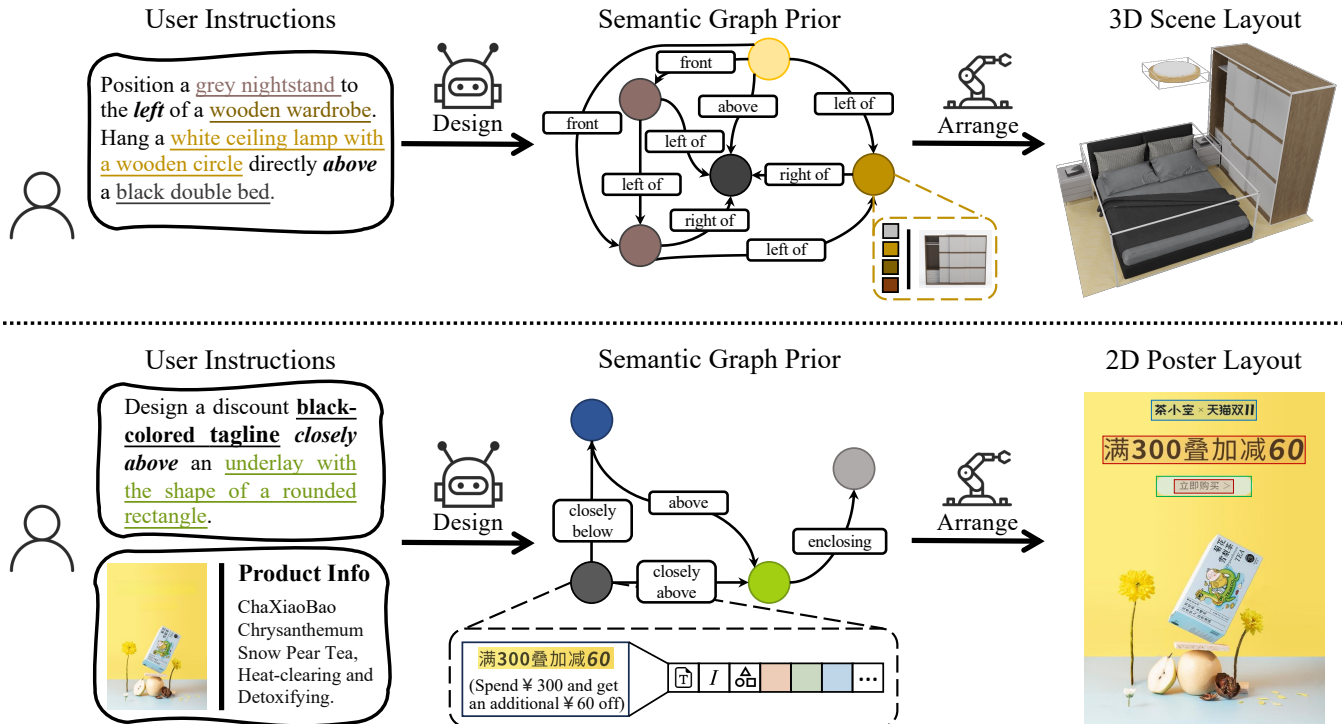


Fig. 1: **Method overview.** For both 3D scene and 2D poster layout synthesis tasks, (1) INSTRUCTLAYOUT first designs a holistic semantic graph based on user instructions. Within the graph, each node is an object endowed with semantic features such as categories and appearances, and each edge represents a spatial relationship between objects. (2) It proceeds to arrange objects in a scene or canvas by decoding spatial attributes from the informative graph prior.

ablation studies.

Our contributions can be summarized as follows:

- We present a unified instruction-driven generative framework for both 3D scene and 2D poster layout synthesis that integrates a semantic graph prior and a layout decoder to improve fidelity and controllability.
- The proposed semantic graph prior jointly models object attributes and layout distributions, facilitating various downstream applications in a zero-shot manner.
- We curate two high-quality datasets to promote the benchmarking of instruction-driven 2D and 3D layout synthesis, and quantitative experiments demonstrate that the proposed method significantly outperforms existing state-of-the-art techniques.

2 RELATED WORK

2.1 3D Scene Layout Synthesis

Graphs have been used to guide complex scene synthesis in the form of scene hierarchies [30; 31], parse trees [32], scene graphs [33; 34], etc. Wang et al. [25] utilize an image-based module and condition its outputs on the edges of a relation graph within each non-differentiable step. They also adopt an autoregressive model [35] to generate relation graphs, which are unconditional and have limited object attributes. Other works [22; 23; 24] adopt conditional VAEs [36; 37] with graph convolutional networks [38] to generate layouts. While offering high controllability, these methods demand the specification of elaborate graph conditions, which are

notably more intricate than those driven by natural languages. With the advent of attention mechanisms [39], recent approaches [16; 17; 20; 21] can implicitly acquire object relations by self-attention and condition scene synthesis with texts by cross-attention. However, text prompts in these works tend to be relatively simple, containing only object categories or lacking layout descriptions, limiting the expressiveness and customization. Implicit relation modeling also significantly hinders their controllability.

2.2 2D Poster Layout Synthesis

Numerous methods have been proposed to automatically synthesize 2D layouts for posters, user interfaces, E-commerce advertisements, etc. Prior research [6; 7; 11; 19; 40] has primarily concentrated on generating layouts from scratch on a blank canvas, while others [10; 12; 18; 41; 42] focus on image content-aware layout synthesis, leading to more practical applications. However, they are either confined to unconditional generation based solely on the canvas (blank or image prior) [6; 7; 41; 42] or relying on object categories [11; 19], lacking the capability to control the layout synthesis process using user-friendly instructions. Furthermore, due to the scarcity of high-quality datasets, only a few studies [12; 43] have delved into predicting 2D object attributes and their textual content, which is vital for generating realistic and informative layouts.

2.3 Generative Models for Graphs

There have been lots of endeavors on generative models for undirected graphs, molecules and scene graphs by autore-

gressive models [44; 45], VAEs [46; 47], GANs [48; 49] and diffusion models [50; 51; 52; 53]. However, none of them is capable of understanding text conditions. Longland et al. [54] and Lo et al. [55] employ VAE and GAN, respectively, for text-driven generation of simple undirected graphs without semantics. We present a pioneering effort to generate holistic semantic graphs with expressive instructions.

3 METHOD

3.1 Problem Statement

Denote $\mathcal{S} := \{\mathcal{S}_1, \dots, \mathcal{S}_M\}$ as a collection of 2D or 3D layouts. Each layout \mathcal{S}_i is composed of multiple objects $\mathcal{O}_i := \{\mathbf{o}_j^i\}_{j=1}^{N_i}$ with distinct attributes $\mathbf{o}_j^i := \{c_j^i, \mathbf{s}_j^i, \mathbf{f}_j^i\}$, including category $c_j^i \in \{1, \dots, K_c\}$, where K_c is the number of object classes in \mathcal{S} , spatial feature \mathbf{s}_j^i , such as scale and location, and semantic feature \mathbf{f}_j^i like appearance and style. To set up a layout, one can generate each object (a 3D model or tagline text) or retrieve it from a database based on c and \mathbf{f} . These objects are then resized and transformed to the expected coordinates by corresponding \mathbf{s} .

Given instructions \mathbf{y} , our goal is to learn the conditional scene distribution $q(\mathcal{S}|\mathbf{y})$. Rather than direct modeling [12; 17; 19; 21], we employ well-structured and informative graphs to serve as general and semantic latent. Each graph \mathcal{G}_i contains a node set $\mathcal{V}_i := \{\mathbf{v}_j^i\}_{j=1}^{N_i}$ and a directed edge set $\mathcal{E}_i := \{e_{jk}^i | \mathbf{v}_j^i, \mathbf{v}_k^i \in \mathcal{V}_i\}$. A node \mathbf{v}_j^i functions as a high-level representation of an object \mathbf{o}_j^i , and a directed edge e_{jk}^i explicitly conveys the relations between objects.

To this end, we propose a generative framework, INSTRUCTLAYOUT, that consists of two components: (1) **semantic graph prior** $p_\phi(\mathcal{G}|\mathbf{y})$ (Sec. 3.3) that jointly models high-level object and relation distributions conditioned on \mathbf{y} ; (2) **layout decoder** $p_\theta(\mathcal{S}|\mathcal{G})$ (Sec. 3.4) that produces precise layout configurations with semantic graphs prior. Since \mathcal{G} is deterministic by corresponding \mathcal{S} , the two networks together yield an instruction-driven generative model for 2D and 3D layouts:

$$p_{\phi, \theta}(\mathcal{S}|\mathbf{y}) = p_{\phi, \theta}(\mathcal{S}, \mathcal{G}|\mathbf{y}) = p_\phi(\mathcal{G}|\mathbf{y})p_\theta(\mathcal{S}|\mathcal{G}). \quad (1)$$

3.2 Preliminary: General Diffusion Models

Diffusion generative models [56] consist of a non-parametric forward process and a learnable reverse process. The forward process progressively corrupts a data point from $q(\mathbf{x}_0)$ to a sequence of increasingly noisy latent variables: $q(\mathbf{x}_{1:T}|\mathbf{x}_0) = \prod_{t=1}^T q(\mathbf{x}_t|\mathbf{x}_{t-1})$. A neural network is trained to reverse the process by denoising them iteratively: $p_\psi(\mathbf{x}_{0:T}|\mathbf{c}) = p(\mathbf{x}_T) \prod_{t=1}^T p_\psi(\mathbf{x}_{t-1}|\mathbf{x}_t, \mathbf{c})$, where \mathbf{c} is an optional condition to guide the reverse process as needed. These two processes are supposed to admit $p(\mathbf{x}_T) \approx q(\mathbf{x}_T|\mathbf{x}_0)$ for a sufficiently large T . The generative model is optimized by minimizing a variational upper bound on $\mathbb{E}_{q(\mathbf{x}_0)} [-\log p_\psi(\mathbf{x}_0)]$:

$$\mathcal{L}_{\text{vb}} := \mathbb{E}_{q(\mathbf{x}_0)} \left[\underbrace{D_{\text{KL}}[q(\mathbf{x}_T|\mathbf{x}_0)||p(\mathbf{x}_T)]}_{\mathcal{L}_T} + \sum_{t=2}^T \mathcal{L}_{t-1} - \underbrace{\mathbb{E}_{q(\mathbf{x}_1|\mathbf{x}_0)} [\log p_\psi(\mathbf{x}_0|\mathbf{x}_1, \mathbf{c})]}_{\mathcal{L}_0} \right], \quad (2)$$

where $\mathcal{L}_{t-1} := D_{\text{KL}}[q(\mathbf{x}_{t-1}|\mathbf{x}_t, \mathbf{x}_0)||p_\psi(\mathbf{x}_{t-1}|\mathbf{x}_t, \mathbf{c})]$ and \mathcal{L}_T is constant during training so can be ignored. $D_{\text{KL}}[\cdot||\cdot]$ indicates the KL divergence between two distributions.

Diffusion models can accommodate both continuous and categorical distributions by a meticulous design of the diffusion kernel $q(\mathbf{x}_t|\mathbf{x}_{t-1})$. A prominent choice for continuous variables is the Gaussian kernel [21; 57; 58]. Uniform transition is widely adopted for categorical variables [52; 59; 60]. In this work, we utilize both the discrete and continuous diffusion models for the two stages in INSTRUCTLAYOUT respectively to model distinct layout attributes.

3.3 Semantic Graph Prior

A semantic graph \mathcal{G} represents an abstract structure of the underlying layout by a node set and an edge set. Each node includes the category c and semantic features \mathbf{f} of an object. Spatial features \mathbf{s} can be derived from relations represented by edges, so we leave them to the decoder $p_\theta(\mathcal{S}|\mathcal{G})$.

3.3.1 Feature Discretization

For the 2D poster layout synthesis task, we consider graphic features, including types of text fonts, italicized or not, and border shapes, which are naturally discrete variables like category. For the colors of text, border, and gradation that are in continuous values, we discretize them in the CIE *Lab* colorspace following Zhang et al. [61] to enhance color saturation and constrain the feature space.

While for the 3D scene layout synthesis task, it's hard to describe geometric shapes and visual appearance of 3D models by explicit categorical attributes, so we utilize a pretrained multimodal-aligned model OpenShape [26] to extract their semantic features. However, these high-dimensional features (e.g., $d = 1280$ in OpenShape `pointbert-vitg14`) are too complicated to model. We circumvent this drawback by introducing a vector-quantized variational autoencoder (VQ-VAE) [62; 63] for feature vectors and quantize each of them by several learnable tokens from the maintained codebook, as depicted in Figure 2(a). The intuition behind it is that 3D models share general intrinsic characteristics, encompassing attributes like colors, materials, and basic geometric shapes. Indexing semantic features in a discrete space achieves a compact feature space for distribution modeling and dramatically reduces the cost of operating in a continuous space.

3.3.2 Discrete Semantic Graph Diffusion

After feature discretization, all attributes in a semantic graph are categorical: a graph $\mathcal{G}_i := (\mathcal{C}_i, \mathcal{F}_i, \mathcal{E}_i)$ with N_i nodes, where $\mathcal{C}_i := \{1, \dots, K_c\}^{N_i}$, $\mathcal{E}_i := \{1, \dots, K_e\}^{N_i \times N_i}$ and $\mathcal{F}_i := \{1, \dots, K_f\}^{N_i \times n_f}$, where n_f is the number of discrete features. While it is possible to embed discrete variables in continuous spaces using one-hot encodings, it diminishes the sparsity inherent in the original data and imposes a substantial burden on network optimization. Instead, we propose to model the semantic graph prior by a **mask-based discrete diffusion model**.

For a scalar discrete random variable with K categories $x \in \{1, \dots, K\}$, diffusion noise is defined by a series of transition matrices $\mathbf{Q} \in \mathbb{R}^{K \times K}$. The forward process at timestep t is expressed as $q(x_t|x_{t-1}) := \mathbf{x}_t^\top \mathbf{Q}_t \mathbf{x}_{t-1}$,

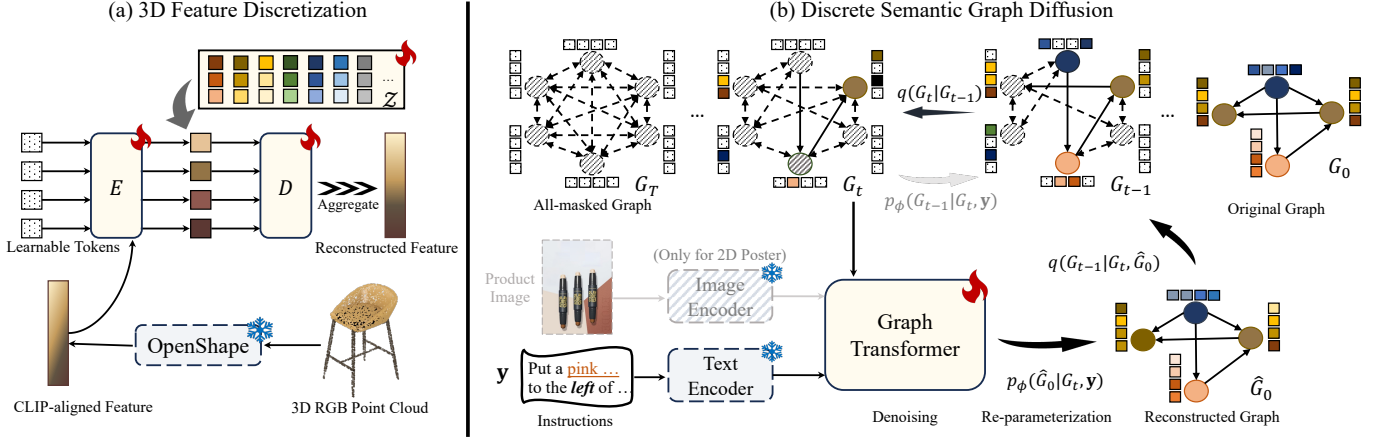


Fig. 2: **Semantic Graph Prior** (Sec. 3.3). (a) **3D Feature Discretization** (Sec. 3.3.1). Unlike the naturally discrete features of 2D poster graphics, semantic features for 3D objects are extracted from a frozen multimodal-aligned model OpenShape and then quantized by codebook entries. (b) **Discrete Semantic Graph Diffusion** (Sec. 3.3.2). Three categorical variables in G_0 are independently diffused; Empty states are not depicted for concision; A graph Transformer with a frozen text encoder and optional image encoder for 2D poster learns the semantic graph prior by iteratively denoising corrupted graphs.

where $\mathbf{x}_t \in \mathbb{R}^K$ is the column one-hot encoding for x_t and $[\mathbf{Q}_t]_{mn} := q(x_t = m | x_{t-1} = n)$ is the probability that x_{t-1} transits to the category m from n . The probabilistic distribution of x_t can be directly derived from x_0 : $q(x_t | x_0) := \mathbf{x}_t^\top \bar{\mathbf{Q}}_t \mathbf{x}_0$, where $\bar{\mathbf{Q}}_t := \mathbf{Q}_t \cdots \mathbf{Q}_1$.

Instead of commonly used Gaussian or uniform transitions for graph generation [50; 51; 52; 59], we propose to diffuse semantic graphs by independently masking graph attributes (i.e., object class c , discrete feature indices f and relation e) by introducing an absorbing state [MASK] [60; 64] to each uniform transition matrix. For object class c , its transition matrix is defined as:

$$\mathbf{Q}_t^c := \begin{bmatrix} \alpha_t^c + \beta_t^c & \beta_t^c & \cdots & \beta_t^c & 0 \\ \beta_t^c & \alpha_t^c + \beta_t^c & \cdots & \beta_t^c & 0 \\ \vdots & \vdots & \ddots & \beta_t^c & 0 \\ \beta_t^c & \beta_t^c & \beta_t^c & \alpha_t^c + \beta_t^c & 0 \\ \gamma_t^c & \gamma_t^c & \gamma_t^c & \gamma_t^c & 1 \end{bmatrix}, \quad (3)$$

by which c_t has a probability of γ_t^c to be masked, a probability of α_t^c to maintain the same, leaving a chance of $1 - \gamma_t^c - \alpha_t^c$ for uniform sampling. [MASK] will always stay in its state. Transition matrices for f and e , denoted as \mathbf{Q}_t^f and \mathbf{Q}_t^e respectively, exhibit analogous structures. Schedules of $(\alpha_t, \beta_t, \gamma_t)$ are designed to admit that the initial states for semantic graphs are all masked.

Since the number of objects varies across different layouts, semantic graphs are padded by empty states to maintain a consistent number of N objects. One-hot encodings for scalar variables c , f and e in a layout are denoted as $\mathbf{C} \in \mathbb{R}^{N \times (K_c + 2)}$, $\mathbf{F} \in \mathbb{R}^{N \times n_f \times (K_f + 2)}$ and $\mathbf{E} \in \mathbb{R}^{N \times N \times (K_e + 2)}$ respectively. Here, “+2” accounts for each variable’s two extra states (i.e., empty state and mask state). A one-hot encoded semantic graph $G_0 := (\mathbf{C}_0, \mathbf{F}_0, \mathbf{E}_0)$ at timestep t is formulated as

$$q(G_t | G_0) = (\bar{\mathbf{Q}}_t^c \mathbf{C}_0, \bar{\mathbf{Q}}_t^f \mathbf{F}_0, \bar{\mathbf{Q}}_t^e \mathbf{E}_0). \quad (4)$$

The process for learning the graph prior is illustrated in Figure 2(b). The independent diffusion with mask states offers two significant advantages:

- Perturbed states for one variable (e.g., \mathbf{C}) could be recovered by incorporating information from uncorrupted portions of the other variables (e.g., \mathbf{F} and \mathbf{E}), compelling the semantic graph prior to learning from the interactions among different scene attributes.
- The introduction of mask states facilitates the distinction between corrupted and clean states, thus simplifying the denoising task.

These benefits are critical, especially for intricate semantic graphs and diverse downstream generative tasks, compared with simple graph generative tasks [50; 51; 52]. An ablation study on the choice of \mathbf{Q} is provided in Sec. 6.2.

The output of the graph prior network is re-parameterized to produce the clean scene graphs \hat{G}_0 , which is then diffused to get the predicted posterior for computing the variational bound in Equation 2: $p_\phi(G_{t-1} | G_t, \mathbf{y}) \propto \sum_{\hat{G}_0} q(G_{t-1} | G_t, \hat{G}_0) p_\phi(\hat{G}_0 | G_t, \mathbf{y})$. Training objective for p_ϕ is a weighted summation of variational bounds for three random variables conditioned on \mathbf{y} :

$$\mathcal{L}_{\text{vb}}^{\mathcal{G}|\mathbf{y}} := \mathcal{L}_{\text{vb}}^{\mathbf{C}|\mathbf{y}} + \lambda_f \cdot \mathcal{L}_{\text{vb}}^{\mathbf{F}|\mathbf{y}} + \lambda_e \cdot \mathcal{L}_{\text{vb}}^{\mathbf{E}|\mathbf{y}}, \quad (5)$$

where λ_e and λ_f are hyperparameters to adjust the relative importance of three components in the semantic graph.

3.4 Layout Decoder

3.4.1 Spatial Feature Generation

Modeling layouts’ spatial features become easy with the semantic graph prior. Spatial features basically include two attributes $\mathbf{s} := \{\mathbf{l}, \mathbf{m}\}$, where $\mathbf{l} \in \mathbb{R}^2$ or \mathbb{R}^3 is the location of an object in 2D or 3D space and $\mathbf{m} \in \mathbb{R}^2$ or \mathbb{R}^3 is its scale. In 3D scenes, an object has an orientation attribute $r \in \mathbb{R}$, allowing it to rotate along the gravity axis. We parameterize the $SO(2)$ rotation by $[\cos(r), \sin(r)]^\top$ to continuously represent r [65]. Consequently, the spatial features of each layout \mathcal{S}_i can be expressed as matrices $\mathbf{L}_i \in \mathbb{R}^{N_i \times d_i}$, where $d_i = 4$ for 2D posters and $d_i = 8$ for 3D scenes. Note that $\mathcal{S} = (\mathbf{L}, \mathcal{G})$, so generating layouts $p_\theta(\mathcal{S} | \mathcal{G})$ is equivalent to

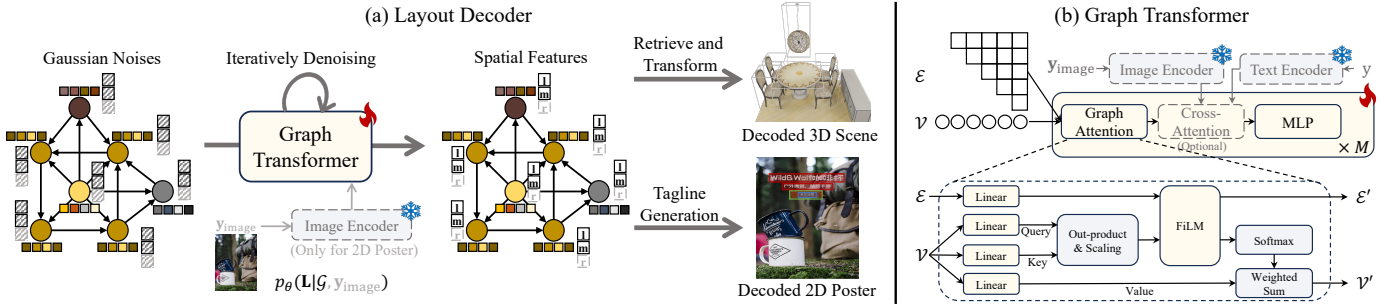


Fig. 3: (a) **Layout Decoder** (Sec. 3.4). Gaussian noises are sampled to attach at every node of semantic graphs; A graph Transformer processes these graphs iteratively to remove noises and generate spatial features (Sec. 3.4.1); A **tagline generator** followed to fill textual contents in each bounding box for 2D poster layout synthesis (Sec. 3.4.2). (b) **Graph Transformer** (Sec. 3.5). A graph Transformer consists of a stack of M blocks, each comprising graph attention, MLP, and optional cross-attention modules for conditions; AdaLN and multihead scheme are not depicted for concision.

learning the conditional distributions of layout configurations $p_{\theta}(\mathbf{L}|\mathcal{G})$. For the 2D layout synthesis task, although spatial relations can be inferred from edges in the semantic graph, we additionally provide clean product poster images y_{image} as conditions for more precise arrangements and to avoid occluding the principal products.

A continuous diffusion model with variance-preserving Gaussian kernels [57; 58] is adopted to learn $p_{\theta}(\mathbf{L}|\mathcal{G})$. Following Ho et al. [57], the variational bound in Equation 2 for the decoder $p_{\theta}(\mathbf{L}|\mathcal{G})$ is reweighted and simplified:

$$\mathcal{L}_{\text{simple}} := \mathbb{E}_{\mathbf{L}_0, t, \epsilon} \|\epsilon - \epsilon_{\theta}(\mathbf{L}_t, t, \mathcal{G})\|^2, \quad (6)$$

where t is sampled from a uniform distribution $\mathcal{U}(1, T)$, ϵ is sampled from a standard normal distribution $\mathcal{N}(\mathbf{0}, \mathbf{I})$ and \mathbf{L}_t is the noised spatial features. A diagram of the layout decoder is depicted in Figure 3(a). Intuitively, the network ϵ_{θ} is trained to predict noise ϵ in \mathbf{L}_t .

3.4.2 Tagline Generation for 2D Poster

After synthesizing semantic features \mathbf{f} and spatial features \mathbf{s} , the pipeline for 3D scene synthesis is completed by retrieving 3D objects from an off-the-shelf dataset based on the generated \mathbf{f} and transforming them to appropriate positions using the generated \mathbf{s} .

For 2D poster synthesis, we proceed to predict the textual contents in bounding boxes using all generated \mathbf{f} and \mathbf{s} associated with user-provided product descriptions and images. Concretely, we primarily adopt the method proposed by Gao et al. [43] to generate tagline captions. This method involves an autoregressive transformer decoder considering multimodal conditions such as background images, product descriptions, and spatial features. A progressive training strategy trains it through two tasks, including caption generation and caption matching. However, the absence of clean product images and semantic features of text bounding boxes results in suboptimal tagline generation. To address this issue, we utilize high-quality cleaned product images processed according to the strategy proposed in Sec. 5.1 and incorporate the generated semantic features from Sec. 3.3 as an additional robust condition to guide generation.

3.5 Model Architecture

The general-purpose Transformer [39] architecture is used for all models across tasks in this work.

Vanilla Transformer. As illustrated in Figure 2(a), n_f learnable tokens are employed with a stack of cross-attentions to extract information from object semantic features \mathbf{f} in the encoder E in VQ-VAE. Regarding the decoder D , n_f vectors retrieved from the codebook \mathcal{Z} are fed to another Transformer, and an average pooling on the top of it is applied to aggregate information.

Graph Transformer. The semantic graph prior and spatial decoder share the same model architecture as shown in Figure 3(b). Since relation e_{jk} can be determined by e_{kj} , only the upper triangular part of the relation matrix is necessary. Object categories and features together form input tokens for Transformers. Message passing on graphs is operated via node self-attention and node-edge fusion with FiLM [66], which linearly modulates edge embeddings and node attention matrices before softmax [52; 67]. Timestep for diffusion t is injected by AdaLN [68; 69]. In the graph prior $p_{\phi}(\mathcal{G}|y)$, instructions and optional product images are embedded by a frozen multimodal encoder CLIP [70] and consistently influence network outputs by cross-attention mechanisms. Layout decoder $p_{\theta}(\mathcal{S}|\mathcal{G})$ is conditioned on semantic graphs by appending sampled Gaussian noises on node embeddings, which are then iteratively denoised to produce layout spatial features.

Permutation Non-invariance. Although \mathcal{G} should ideally remain invariant to node permutations, invariant diffusion models could encounter learning challenges for multi-mode modeling. Thus, each node feature is added with positional encodings [21; 39; 71] before the permutation-equivariant Transformer. Exchangeability for graph prior distributions is strived by random permutation augmentation during the training process. Ablation on the permutation non-invariance is provided in Sec. 6.2.

4 INSTRUCTLAYOUT FOR 3D SCENE SYNTHESIS

4.1 3D Indoor Scene-Instruction Paired Dataset

All experiments are conducted on 3D-FRONT [72], a professionally designed collection of synthetic indoor scenes. However, it does not contain any descriptions of room

TABLE 1: Quantitive evaluations for instruction-driven synthesis 3D indoor scene by ATISS [17], DiffuScene [21] and our method on three room types. Higher iRecall, lower FID, FID^{CLIP} , and KID indicate better synthesis quality. For SCA, a score closer to 50% is better. Standard deviation values are provided as subscripts.

3D Instruction-driven Synthesis		\uparrow iRecall%	\downarrow FID	\downarrow FID^{CLIP}	\downarrow KID $\times 1e-3$	SCA%
Bedroom	ATISS	48.13 \pm 2.50	119.73 \pm 1.55	6.95 \pm 0.06	0.39 \pm 0.02	59.17 \pm 1.39
	DiffuScene	56.43 \pm 2.07	123.09 \pm 0.79	7.13 \pm 0.16	0.39 \pm 0.01	60.49 \pm 2.96
	Ours	73.64\pm1.37	114.78\pm1.19	6.65\pm0.18	0.32\pm0.03	56.02\pm1.43
Living room	ATISS	29.50 \pm 3.67	117.67 \pm 2.32	6.08 \pm 0.13	17.60 \pm 2.65	69.38 \pm 3.38
	DiffuScene	31.15 \pm 2.49	122.20 \pm 1.09	6.10 \pm 0.11	16.49 \pm 1.24	72.92 \pm 1.29
	Ours	56.81\pm2.85	110.39\pm0.78	5.37\pm0.07	8.16\pm0.56	65.42\pm2.52
Dining room	ATISS	37.58 \pm 1.99	137.10 \pm 0.34	8.49 \pm 0.23	23.60 \pm 2.52	67.61 \pm 3.23
	DiffuScene	37.87 \pm 2.76	145.48 \pm 1.36	8.63 \pm 0.31	24.08 \pm 1.90	70.57 \pm 2.14
	Ours	61.23\pm1.67	129.76\pm1.61	7.67\pm0.18	13.24\pm1.79	64.20\pm1.90

TABLE 2: Quantitive evaluations for zero-shot generative applications on three room types. ‘‘Uncond.’’ stands for unconditional scene synthesis.

Zero-shot Applications		Stylization		Re-arrangement		Completion		Uncond.
		$\uparrow \Delta_{\times 1e-3}$	\downarrow FID	\uparrow iRecall%	\downarrow FID	\uparrow iRecall%	\downarrow FID	\downarrow FID
Bedroom	ATISS	3.44	123.91	61.22	107.67	64.90	89.77	134.51
	DiffuScene	1.08	127.35	68.57	106.15	48.57	96.28	135.46
	Ours	6.34	122.73	79.59	105.27	69.80	82.98	124.97
Living room	ATISS	-3.57	110.85	31.97	117.97	43.20	106.48	129.23
	DiffuScene	-2.69	112.80	41.50	115.30	19.73	95.94	129.75
	Ours	0.28	109.39	56.12	106.85	46.94	92.52	117.62
Dining room	ATISS	-1.11	131.14	36.06	134.54	57.99	122.44	147.52
	DiffuScene	-2.98	135.20	46.84	133.73	32.34	115.08	150.81
	Ours	1.69	128.78	62.08	125.07	60.59	107.86	137.52

layouts or object appearances. To construct a high-quality scene-instruction paired dataset, we initially extract view-dependent spatial relations with predefined rules [22; 38]. The dataset is further enhanced by captioning objects with BLIP [27]. To ensure the accuracy of descriptions, the generated captions are filtered by ChatGPT [28; 29] with object ground-truth categories. The final instructions are derived from randomly selected relation triplets. Verbs and conjunctions in the sentences are also randomly picked to keep the diversity and fluency of prompts. Details on 3D dataset curation can be found in Appendix A.1.

4.2 Experiments Settings

4.2.1 Baselines

We compare our method with two state-of-the-art approaches for the 3D scene synthesis tasks:

- **ATISS** [17], a Transformer-based auto-regressive network that regards scenes as sets of unordered objects and generates objects and their attributes sequentially.
- **DiffuScene** [21], a continuous diffusion model with Gaussian kernels that treats object attributes in one scene as a 2D matrix after padding them to a fixed size.

Both methods can be conditioned on text prompts by cross-attention with a pretrained text encoder. Our preliminary experiments suggest that both baselines encounter difficulties in modeling high-dimensional semantic feature

distributions, consequently impacting their performance in generating other attributes. Therefore, we augment them to generate quantized features.

4.2.2 Evaluation Metrics

To assess the controllability of layouts, we use a metric named ‘‘instruction recall’’ (**iRecall**), which quantifies the proportion of the required triplets ‘‘(subject, relation, object)’’ occurring in synthesized scenes to all provided in instructions. It is a stringent metric that simultaneously considers all three elements in a layout relation. Following previous works [17; 20; 21], we also report Fréchet Inception Distance (**FID**) [73], FID^{CLIP} [74], which computes FID scores by CLIP features [70], Kernel Inception Distance (**KID**) [75], scene classification accuracy (**SCA**). These metrics evaluate the overall quality of synthesized scenes and rely on rendered images. We use Blender [76] to produce high-quality images for both synthesized and real scenes.

4.3 Instruction-drive 3D Scene Synthesis

Table 1 presents the quantitive evaluations for synthesizing 3D scenes with instructions. We report the average scores of five runs with different random seeds. As demonstrated, even with the enhancement of quantized semantic features, two baseline methods continue to demonstrate inferior performance compared to ours. ATISS outperforms DiffuScene

regarding generation fidelity, owing to its capacity to model in discrete spaces. DiffuScene shows better controllability to ATISS because it affords global visibility of samples during generation. Our proposed INSTRUCTLAYOUT exhibits the best of both worlds. Remarkably, we achieve a substantial advancement in controllability, measured in iRecall, for scene generative models, surpassing current state-of-the-art approaches by about 15%~25% across various room types, all while maintaining high fidelity. It is noteworthy that INSTRUCTLAYOUT excels in handling more complex scenes, such as living and dining rooms, which typically comprise an average of 20 objects, in contrast to bedrooms, which have only 8 objects on average, revealing the benefits of modeling intricate 3D scenes associated with the semantic graph prior. Qualitative visualizations are provided in Appendix B.1.

4.4 Zero-shot Applications

Thanks to the discrete design and mask modeling, the learned semantic graph prior can perform diverse downstream tasks without any fine-tuning. We investigate four zero-shot tasks: **stylization**, **re-arrangement**, **completion**, and **unconditional generation**.

Stylization and re-arrangement task can be formulated as $p_\phi(\mathbf{f}|c, \mathbf{s}, \mathbf{y})$ and $p_{\phi, \theta}(\mathbf{s}|c, \mathbf{f}, \mathbf{y})$ respectively. In the completion task, we intend to add new objects $\{\mathbf{o}_k^i\}$ to a partial scene \mathcal{S}_i with instructions. By filling the partial scene attributes with [MASK] tokens, we treat them as intermediate states during discrete graph denoising, allowing for a straightforward adaptation of the learned semantic graph prior to these tasks in a zero-shot manner. Unconditional synthesis is implemented by simply setting instruction embeddings \mathbf{y} as zeros. To assess controllability in the stylization task, we define $\Delta := \frac{1}{N} \sum_{i=1}^N \text{CosSim}(\mathbf{f}_i, \mathbf{d}_i^{\text{style}}) - \text{CosSim}(\mathbf{f}_i, \mathbf{d}_i^{\text{class}})$, where $\mathbf{d}_i^{\text{style}}$ represents the CLIP text feature of object class name with the desired style, and $\mathbf{d}_i^{\text{class}}$ is the CLIP text feature with only class information. $\text{CosSim}(\cdot, \cdot)$ calculates the cosine similarity between two vectors.

Evaluations on zero-shot applications are reported in Table 2. Our method consistently outperforms two strong baselines in both controllability and fidelity. While ATISS, as an auto-regressive model, is a natural fit for the completion task, its unidirectional dependency chain limits its effectiveness for tasks requiring global scene modeling, such as re-arrangement. DiffuScene can adapt to these tasks by replacing the known parts with the noised corresponding scene attributes during sampling, similar to image inpainting [77; 78]. However, the known attributes are greatly corrupted in the early steps, which could misguide the denoising direction and necessitate fine-tuning. Additionally, DiffuScene also faces challenges in searching for semantic features in a continuous space for stylization. In contrast, INSTRUCTLAYOUT globally models scene attributes and treats partial scene attributes as intermediate discrete states during training. These designs effectively eliminate the training-test gap, rendering it highly versatile for a wide range of downstream tasks. Visualizations of zero-shot applications are available in Appendix B.2.

5 INSTRUCTLAYOUT FOR 2D POSTER SYNTHESIS

5.1 2D E-commerce Poster-Instruction Paired Dataset

AutoPoster [12] is a recently proposed public poster dataset containing 76,537 E-commerce posters with detailed annotations of layout elements. Compared with an ideal comprehensive poster design pipeline, however, it lacks three essential components, including (1) design instructions describing the desired layout of a poster, (2) principle product descriptions for tagline generation, and (3) clean product images for use as poster backgrounds. To the best of our knowledge, no existing dataset offers comprehensive information for the instruction-driven poster synthesis task [10; 41; 43].

In this work, we bridge this gap by constructing a high-quality 2D E-commerce poster dataset based on the AutoPoster dataset. Similar to 3D scene dataset curation, we use predefined rules as a systematic instruction generation pipeline and collect 73,070 product descriptions for AutoPoster posters from public Internet sources using web crawler techniques. For clean product images, previous works[10; 12] employ an off-the-shelf inpainting model LaMa [79] to remove the graphics elements from the poster. However, LaMa often struggles with posters featuring frequent and significant color shifts, resulting in blurry and unnatural distortion of the processed product images. To mitigate this, we first mask out graphic elements with the average color near the masked region and then apply the LaMa inpainting model to obtain clean product images. More details on the 2D poster dataset curation are provided in Appendix A.2.

5.2 Experiments Settings

5.2.1 Baselines

We re-implemented several state-of-the-art 2D layout synthesis models for a comprehensive comparison:

- **LayoutTransformer** [6], a Transformer decoder that simultaneously predicts categories and discretizes sizes autoregressively.
- **LayoutVAE** [7], a VAE-based model that autoregressively predicts the conditional distribution of elements' counts and bounding boxes.
- **DS-GAN** [10], a GAN-based model that builds a Design Sequence GAN and generates layouts with product images in a specially designed order.
- **DDPM** [57], a native continuous diffusion model, and we modify it to enable simultaneous prediction of categories and bound boxes.
- **LayoutDM** [19], a single-stage discrete diffusion model that discretizes layout attributes and diffuses them in a discrete space.
- **SAP** [12], a Transformer encoder designed for graphic semantic feature synthesis with conditions of product images and layout bounding boxes.

During the re-implementation process, we further condition these baselines with product images and text prompts. While DS-GAN [10] fails to converge with textual instructions, we only feed image conditions to it. Note that most of these methods [6; 7; 10; 19; 57] can only generate categories c and spatial features \mathbf{s} , and SAP [12] only predict graphic semantic features \mathbf{f} .

TABLE 3: Quantitive evaluations for instruction-driven 2D poster synthesis on baselines [6; 7; 10; 19] and INSTRUCTLAYOUT. Higher iRecall, Val, Und_l and Und_s, and lower Ove, N-Ali, and Occ indicate better generation quality. The best results among different models are bolded. Standard deviation values are provided as subscripts.

2D Instruction-driven Synthesis	↑ iRecall%	↑ Val%	↓ Ove _{×100}	↓ N-Ali _{×100}	↑ Und _l %	↑ Und _s %	↓ Occ%
LayoutTransformer [6]	65.689±0.83	98.651±0.07	0.855±0.06	0.324±0.04	95.083±0.18	84.888±0.28	7.742±0.05
LayoutVAE [7]	19.002±0.57	94.877±0.10	8.437±0.06	5.261±0.10	91.195±0.25	82.620±0.35	15.918±0.03
DS-GAN [10] (No Instruction)	\	82.385±0.42	2.072±0.11	0.225±0.01	85.933±0.64	47.115±0.75	8.537±0.41
DDPM [57]	20.986±0.50	94.782±0.23	17.573±0.45	5.980±0.21	63.587±0.56	57.908±0.56	11.868±0.20
LayoutDM [19]	62.999±1.62	93.008±0.24	2.500±0.11	0.240±0.02	86.965±0.36	82.454±0.42	7.242±0.04
Ours	78.451±0.294	99.977±0.01	0.785±0.02	0.165±0.01	97.123±0.15	92.490±0.29	6.565±0.05

TABLE 4: Quantitive evaluations for generated semantic features on SAP [12] and INSTRUCTLAYOUT. “D”, “G”, and “S” represent dominant, gradient, and stroke colors, respectively. Lower MAE and MSE indicate better results.

2D Graphic Features	↓ D-ab(MSE)	↓ D-light(MAE)	↓ S-ab(MSE)	↓ S-light(MAE)	↓ G-ab(MSE)	↓ G-light(MAE)
Random	78.411	5.946	76.062	6.146	80.536	6.596
SAP [12]	74.501	4.197	55.201	2.920	72.369	3.368
Ours	31.047	2.459	33.005	2.872	41.067	1.745

5.2.2 Evaluation Metrics

Besides iRecall proposed in Sec. 4.2.2 to measure the controllability of layout synthesis, we adopt several graphic and content-aware metrics following previous works [10; 41; 42]. Graphic metrics measure the degree of visual harmony among elements (texts, underlay and logos), including Validity (Val) measuring the validity rate of all predicted elements, Overlay (Ove) representing the average Intersection over Union (IoU) for each pair of elements except underlays, Non-Alignment (N-Ali) measuring the extent of spatial non-alignment, and Underlay-Effectiveness (Und_l and Und_s) indicating the quality of generated underlay. For the content-aware metric, we use Occlusion (Occ) to evaluate the overall visual impact of the poster by measuring the degree of occlusion of the background subject by elements. For semantic feature quality assessment, we follow Lin et al. [12] to calculate the accuracy of predicted dominant colors, stroke colors, and gradient colors in Lab space using Mean Squared Error (MSE) and Mean Absolute Error (MAE).

5.3 Instruction-drive 2D Poster Synthesis

Table 3 shows quantitive evaluations on 2D layout generation. We run all models with 5 different random seeds and report the average score. INSTRUCTLAYOUT considerably outperforms other existing models by a large margin among all metrics. Especially, our two-stage diffusion model, which skillfully combines discrete and continuous features, remarkably beats both the single-stage diffusion models, the continuous DDPM [57] and the discrete LayoutDM [19], in terms of controllability and visual harmony. It highlights the effectiveness of the proposed discrete graph prior and the capacity of modeling fine spatial relationships facilitated by the continuous diffusion process in the second stage. As presented in Table 4, INSTRUCTLAYOUT is also capable of leveraging both image and positional information to mimic the behavior of human designers better and generate graphic semantic features of higher usability. Qualitative

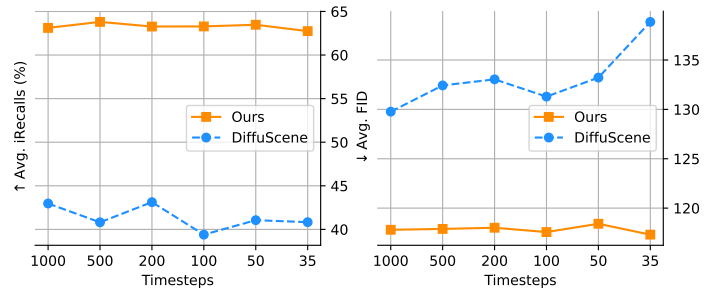


Fig. 4: Ablation study on timesteps for diffusion models on 3D scene layout synthesis task.

results of generated posters with textual content synthesized by the tagline generator are provided in Appendix B.3.

6 ABLATION STUDY

6.1 Diffusion Timesteps

Although containing two diffusion models, our method could achieve better efficiency by reducing the steps of reverse processes without a noticeable decline in performance. We compare INSTRUCTLAYOUT with DiffuScene [21] and LayoutDM [19] in Figure 4 and Table 5 for 3D scene and 2D poster layout synthesis tasks respectively. We try different timesteps T such as “100+100”, “100+10”, and “25+10”, where the first number represents timesteps for semantic graph prior and the latter is for layout decoder. We find that $T = 100$ and 10 is sufficient for $p_\phi(\mathcal{G}|y)$ and $p_\theta(\mathcal{S}|\mathcal{G})$ respectively. This stems from the fact that each stage in INSTRUCTLAYOUT tackles an easier denoising task compared to single-stage diffusion models such as DiffuScene [21] and LayoutDM [11].

6.2 Learning Semantic Graph Prior

We then explore different strategies to learn semantic graph prior. All experiments are conducted on the 3D bedroom dataset. Quantitative results are presented in Table 6.

TABLE 5: Ablation study on diffusion timesteps on 2D poster layout synthesis task.

2D Timestep Ablation	\uparrow iRecall%	\uparrow Val%	\downarrow Ove $\times 100$	\downarrow N-Ali $\times 100$	\uparrow Und $_t$ %	\uparrow Und $_s$ %	\downarrow Occ%
LayoutDM ($T = 110$)	65.841	93.003	2.350	0.222	86.872	82.183	7.236
LayoutDM ($T = 60$)	64.293	92.467	2.532	0.279	86.213	81.902	7.293
LayoutDM ($T = 35$)	61.825	90.145	2.813	0.468	81.911	75.312	7.470
Ours ($T = 100 + 10$)	78.268	99.995	0.992	0.193	96.067	89.285	6.587
Ours ($T = 50 + 10$)	78.833	99.995	1.151	0.188	95.537	88.560	6.580
Ours ($T = 25 + 10$)	77.862	99.986	1.186	0.192	94.277	86.225	6.662

TABLE 6: Ablation study on different strategies to learn semantic graph prior $p_\phi(\mathcal{G}|\mathbf{y})$. "Perm. Invar." means permutation-invariant graph modeling.

Graph Prior	Ours	Gaussian	Joint Mask	Uniform	Perm. Invar.
\uparrow iRecall%	73.64 ± 1.37	34.18 ± 2.53	34.21 ± 2.79	69.22 ± 3.25	70.49 ± 2.50
\downarrow FID	114.78 ± 1.19	128.98 ± 0.97	130.86 ± 2.76	139.61 ± 1.06	116.53 ± 1.35
\downarrow FID ^{CLIP}	6.65 ± 0.18	7.30 ± 0.03	7.59 ± 0.17	8.82 ± 0.24	6.69 ± 0.16
\downarrow KID $\times 1e^{-3}$	0.32 ± 0.03	2.63 ± 0.73	4.82 ± 1.69	10.55 ± 1.19	0.37 ± 0.02
SCA%	56.02 ± 0.91	57.10 ± 3.22	60.37 ± 3.13	76.79 ± 3.14	58.64 ± 1.33

Transition Matrices for Learning Graph Prior. We investigate the effects of different transition matrices for learning the proposed semantic graph prior, including: (1) Embed all categorical variables into their one-hot encodings and diffuse them by Gaussian kernels, which is similar to Niu et al. [50] and Jo et al. [51]; (2) Jointly masking \mathbf{F} and \mathbf{E} along with nodes \mathbf{C} in a graph, so only the attributes of other objects can be utilized for recovery; (3) Adopt uniform transition matrices without mask states, similar to Vignac et al. [52]. Evaluations on both controllability and fidelity reveal the advantages of our independent mask strategy.

Permutation Non-invariance. Different to previous studies on graph generation [50; 51; 52], we depart from the permutation-invariant modeling convention to ease the semantic graph prior learning process. We strive to preserve exchangeable graph distributions by randomly shuffling object orders during training. Performance for invariant graph prior is provided in the last column of Table 6. Its performance declines due to the unnecessary imposition of invariance in scene synthesis.

7 CONCLUSION

By integrating a semantic graph prior and a layout decoder, we propose a novel generative framework, INSTRUCTLAYOUT, that significantly improves the controllability and fidelity of 2D and 3D layout synthesis, providing a user-friendly interface through instructions in natural languages. Benefiting from the design of semantic graph prior, our method can also apply to diverse applications without any fine-tuning. The controllability and versatility positions INSTRUCTLAYOUT as a promising tool. Meanwhile, given the rapid development of large language models (LLMs), integrating an LLM into our instruction-driven pipeline holds significant promise for further enhancing generation interactivity. We hope this work can help in practical scenarios, such as streamlining e-commerce poster design and

facilitating interior design, and serves as a good starting point for creating high-quality instruction datasets in 2D poster and 3D scene applications.

REFERENCES

- [1] P. Merrell, E. Schkufza, Z. Li, M. Agrawala, and V. Koltun, "Interactive furniture layout using interior design guidelines," *ACM Transactions on Graphics (TOG)*, vol. 30, no. 4, pp. 1–10, 2011.
- [2] M. Fisher, M. Savva, Y. Li, P. Hanrahan, and M. Nießner, "Activity-centric scene synthesis for functional 3d scene modeling," *ACM Transactions on Graphics (TOG)*, vol. 34, no. 6, pp. 1–13, 2015.
- [3] S. Qi, Y. Zhu, S. Huang, C. Jiang, and S.-C. Zhu, "Human-centric indoor scene synthesis using stochastic grammar," in *Proceedings of the IEEE Conference on Computer Vision and Pattern Recognition (CVPR)*, 2018, pp. 5899–5908.
- [4] D. Ritchie, K. Wang, and Y.-a. Lin, "Fast and flexible indoor scene synthesis via deep convolutional generative models," in *Proceedings of the IEEE/CVF Conference on Computer Vision and Pattern Recognition (CVPR)*, 2019, pp. 6182–6190.
- [5] Z. Zhang, Z. Yang, C. Ma, L. Luo, A. Huth, E. Vouga, and Q. Huang, "Deep generative modeling for scene synthesis via hybrid representations," *ACM Transactions on Graphics (TOG)*, vol. 39, no. 2, pp. 1–21, 2020.
- [6] K. Gupta, J. Lazarow, A. Achille, L. S. Davis, V. Mahadevan, and A. Shrivastava, "Layouttransformer: Layout generation and completion with self-attention," in *Proceedings of the IEEE/CVF International Conference on Computer Vision (ICCV)*, 2021, pp. 1004–1014.
- [7] A. A. Jyothis, T. Durand, J. He, L. Sigal, and G. Mori, "Layoutvae: Stochastic scene layout generation from a label set," in *Proceedings of the IEEE/CVF International Conference on Computer Vision (ICCV)*, 2019.

- [8] M.-J. Yang, Y.-X. Guo, B. Zhou, and X. Tong, "Indoor scene generation from a collection of semantic-segmented depth images," in *Proceedings of the IEEE/CVF International Conference on Computer Vision (ICCV)*, 2021, pp. 15 203–15 212.
- [9] L. Höllein, A. Cao, A. Owens, J. Johnson, and M. Nießner, "Text2room: Extracting textured 3d meshes from 2d text-to-image models," in *Proceedings of the IEEE/CVF International Conference on Computer Vision (ICCV)*, 2023, pp. 7909–7920.
- [10] H. Y. Hsu, X. He, Y. Peng, H. Kong, and Q. Zhang, "Posterlayout: A new benchmark and approach for content-aware visual-textual presentation layout," in *Proceedings of the IEEE/CVF Conference on Computer Vision and Pattern Recognition (CVPR)*, 2023, pp. 6018–6026.
- [11] S. Chai, L. Zhuang, and F. Yan, "Layoutdm: Transformer-based diffusion model for layout generation," in *Proceedings of the IEEE/CVF Conference on Computer Vision and Pattern Recognition (CVPR)*, 2023, pp. 18 349–18 358.
- [12] J. Lin, M. Zhou, Y. Ma, Y. Gao, C. Fei, Y. Chen, Z. Yu, and T. Ge, "Autoposter: A highly automatic and content-aware design system for advertising poster generation," in *Proceedings of the 31st ACM International Conference on Multimedia (ACM MM)*, 2023, pp. 1250–1260.
- [13] L. Song, L. Cao, H. Xu, K. Kang, F. Tang, J. Yuan, and Y. Zhao, "Roomdreamer: Text-driven 3d indoor scene synthesis with coherent geometry and texture," *arXiv preprint arXiv:2305.11337*, 2023.
- [14] W. Feng, W. Zhu, T.-J. Fu, V. Jampani, A. R. Akula, X. He, S. Basu, X. E. Wang, and W. Y. Wang, "LayoutGPT: Compositional visual planning and generation with large language models," in *Advances in Neural Information Processing Systems (NeurIPS)*, 2023.
- [15] A. G. Patil, S. G. Patil, M. Li, M. Fisher, M. Savva, and H. Zhang, "Advances in data-driven analysis and synthesis of 3d indoor scenes," *Computer Graphics Forum*, 2023.
- [16] X. Wang, C. Yeshwanth, and M. Nießner, "Sceneformer: Indoor scene generation with transformers," in *International Conference on 3D Vision (3DV)*, 2021, pp. 106–115.
- [17] D. Paschalidou, A. Kar, M. Shugrina, K. Kreis, A. Geiger, and S. Fidler, "Atiss: Autoregressive transformers for indoor scene synthesis," *Advances in Neural Information Processing Systems (NeurIPS)*, vol. 34, pp. 12 013–12 026, 2021.
- [18] Y. Cao, Y. Ma, M. Zhou, C. Liu, H. Xie, T. Ge, and Y. Jiang, "Geometry aligned variational transformer for image-conditioned layout generation," in *Proceedings of the 30th ACM International Conference on Multimedia (ACM MM)*, 2022, pp. 1561–1571.
- [19] N. Inoue, K. Kikuchi, E. Simo-Serra, M. Otani, and K. Yamaguchi, "Layoutdm: Discrete diffusion model for controllable layout generation," in *Proceedings of the IEEE/CVF Conference on Computer Vision and Pattern Recognition (CVPR)*, 2023, pp. 10 167–10 176.
- [20] J. Liu, W. Xiong, I. Jones, Y. Nie, A. Gupta, and B. Oğuz, "Clip-layout: Style-consistent indoor scene synthesis with semantic furniture embedding," *arXiv preprint arXiv:2303.03565*, 2023.
- [21] J. Tang, Y. Nie, L. Markhasin, A. Dai, J. Thies, and M. Nießner, "Diffuscene: Scene graph denoising diffusion probabilistic model for generative indoor scene synthesis," in *Proceedings of the IEEE/CVF Conference on Computer Vision and Pattern Recognition (CVPR)*, 2024.
- [22] A. Luo, Z. Zhang, J. Wu, and J. B. Tenenbaum, "End-to-end optimization of scene layout," in *Proceedings of the IEEE/CVF Conference on Computer Vision and Pattern Recognition (CVPR)*, 2020, pp. 3754–3763.
- [23] H. Dharmo, F. Manhardt, N. Navab, and F. Tombari, "Graph-to-3d: End-to-end generation and manipulation of 3d scenes using scene graphs," in *Proceedings of the IEEE/CVF International Conference on Computer Vision (ICCV)*, 2021, pp. 16 352–16 361.
- [24] G. Zhai, E. P. Örnek, S.-C. Wu, Y. Di, F. Tombari, N. Navab, and B. Busam, "Commonscenes: Generating commonsense 3d indoor scenes with scene graphs," *Advances in Neural Information Processing Systems (NeurIPS)*, 2023.
- [25] K. Wang, Y.-A. Lin, B. Weissmann, M. Savva, A. X. Chang, and D. Ritchie, "Planit: Planning and instantiating indoor scenes with relation graph and spatial prior networks," *ACM Transactions on Graphics (TOG)*, vol. 38, no. 4, pp. 1–15, 2019.
- [26] M. Liu, R. Shi, K. Kuang, Y. Zhu, X. Li, S. Han, H. Cai, F. Porikli, and H. Su, "Openshape: Scaling up 3d shape representation towards open-world understanding," *Advances in Neural Information Processing Systems (NeurIPS)*, 2023.
- [27] J. Li, D. Li, C. Xiong, and S. Hoi, "Blip: Bootstrapping language-image pre-training for unified vision-language understanding and generation," in *International Conference on Machine Learning (ICML)*, 2022, pp. 12 888–12 900.
- [28] L. Ouyang, J. Wu, X. Jiang, D. Almeida, C. Wainwright, P. Mishkin, C. Zhang, S. Agarwal, K. Slama, A. Ray *et al.*, "Training language models to follow instructions with human feedback," *Advances in Neural Information Processing Systems (NeurIPS)*, vol. 35, pp. 27 730–27 744, 2022.
- [29] OpenAI, "Gpt-4 technical report," *arXiv preprint arXiv:2303.08774*, 2023.
- [30] M. Li, A. G. Patil, K. Xu, S. Chaudhuri, O. Khan, A. Shamir, C. Tu, B. Chen, D. Cohen-Or, and H. Zhang, "Grains: Generative recursive autoencoders for indoor scenes," *ACM Transactions on Graphics (TOG)*, vol. 38, no. 2, pp. 1–16, 2019.
- [31] L. Gao, J.-M. Sun, K. Mo, Y.-K. Lai, L. J. Guibas, and J. Yang, "Scenehgn: Hierarchical graph networks for 3d indoor scene generation with fine-grained geometry," *IEEE Transactions on Pattern Analysis and Machine Intelligence (T-PAMI)*, 2023.
- [32] P. Purkait, C. Zach, and I. Reid, "Sg-vae: Scene grammar variational autoencoder to generate new indoor scenes," in *European Conference on Computer Vision (ECCV)*, 2020, pp. 155–171.
- [33] Y. Zhou, Z. While, and E. Kalogerakis, "Scenegraphnet: Neural message passing for 3d indoor scene augmentation," in *Proceedings of the IEEE/CVF International Conference on Computer Vision (ICCV)*, 2019, pp. 7384–7392.

- [34] W. Para, P. Guerrero, T. Kelly, L. J. Guibas, and P. Wonka, "Generative layout modeling using constraint graphs," in *Proceedings of the IEEE/CVF International Conference on Computer Vision (ICCV)*, 2021, pp. 6690–6700.
- [35] Y. Li, O. Vinyals, C. Dyer, R. Pascanu, and P. Battaglia, "Learning deep generative models of graphs," *arXiv preprint arXiv:1803.03324*, 2018.
- [36] D. P. Kingma and M. Welling, "Auto-encoding variational bayes," in *International Conference on Learning Representations (ICLR)*, 2014.
- [37] K. Sohn, H. Lee, and X. Yan, "Learning structured output representation using deep conditional generative models," *Advances in Neural Information Processing Systems (NeurIPS)*, vol. 28, 2015.
- [38] J. Johnson, A. Gupta, and L. Fei-Fei, "Image generation from scene graphs," in *Proceedings of the IEEE Conference on Computer Vision and Pattern Recognition (CVPR)*, 2018, pp. 1219–1228.
- [39] A. Vaswani, N. Shazeer, N. Parmar, J. Uszkoreit, L. Jones, A. N. Gomez, Ł. Kaiser, and I. Polosukhin, "Attention is all you need," *Advances in Neural Information Processing Systems (NeurIPS)*, vol. 30, 2017.
- [40] K. Kikuchi, E. Simo-Serra, M. Otani, and K. Yamaguchi, "Constrained graphic layout generation via latent optimization," in *Proceedings of the 29th ACM International Conference on Multimedia (ACM MM)*, 2021.
- [41] M. Zhou, C. Xu, Y. Ma, T. Ge, Y. Jiang, and W. Xu, "Composition-aware graphic layout gan for visual-textual presentation designs," *arXiv preprint arXiv:2205.00303*, 2022.
- [42] C. Xu, M. Zhou, T. Ge, Y. Jiang, and W. Xu, "Unsupervised domain adaption with pixel-level discriminator for image-aware layout generation," in *Proceedings of the IEEE/CVF Conference on Computer Vision and Pattern Recognition (CVPR)*, 2023, pp. 10 114–10 123.
- [43] Y. Gao, X. Hou, Y. Zhang, T. Ge, Y. Jiang, and P. Wang, "Caponimage: Context-driven dense-captioning on image," in *Proceedings of the 2022 Conference on Empirical Methods in Natural Language Processing (EMNLP)*, 2022, pp. 3449–3465.
- [44] J. You, R. Ying, X. Ren, W. Hamilton, and J. Leskovec, "Graphrnn: Generating realistic graphs with deep autoregressive models," in *International Conference on Machine Learning (ICML)*, 2018, pp. 5708–5717.
- [45] S. Garg, H. Dhama, A. Farshad, S. Musatian, N. Navab, and F. Tombari, "Unconditional scene graph generation," in *Proceedings of the IEEE/CVF International Conference on Computer Vision (ICCV)*, 2021, pp. 16 362–16 371.
- [46] M. Simonovsky and N. Komodakis, "Graphvae: Towards generation of small graphs using variational autoencoders," in *International Conference on Artificial Neural Networks (ICANN)*, 2018, pp. 412–422.
- [47] T. Verma, A. De, Y. Agrawal, V. Vinay, and S. Chakrabarti, "Varscene: A deep generative model for realistic scene graph synthesis," in *International Conference on Machine Learning (ICML)*, 2022, pp. 22 168–22 183.
- [48] N. De Cao and T. Kipf, "MolGAN: An implicit generative model for small molecular graphs," *ICML 2018 workshop on Theoretical Foundations and Applications of Deep Generative Models*, 2018.
- [49] K. Martinkus, A. Loukas, N. Perraudin, and R. Wattenhofer, "Spectre: Spectral conditioning helps to overcome the expressivity limits of one-shot graph generators," in *International Conference on Machine Learning (ICML)*, 2022, pp. 15 159–15 179.
- [50] C. Niu, Y. Song, J. Song, S. Zhao, A. Grover, and S. Ermon, "Permutation invariant graph generation via score-based generative modeling," in *International Conference on Artificial Intelligence and Statistics (AISTATS)*, 2020, pp. 4474–4484.
- [51] J. Jo, S. Lee, and S. J. Hwang, "Score-based generative modeling of graphs via the system of stochastic differential equations," in *International Conference on Machine Learning (ICML)*, 2022, pp. 10 362–10 383.
- [52] C. Vignac, I. Krawczuk, A. Siraudin, B. Wang, V. Cevher, and P. Frossard, "Digress: Discrete denoising diffusion for graph generation," in *International Conference on Learning Representations (ICLR)*, 2023.
- [53] L. Kong, J. Cui, H. Sun, Y. Zhuang, B. A. Prakash, and C. Zhang, "Autoregressive diffusion model for graph generation," in *International Conference on Machine Learning (ICML)*, vol. 202, 2023, pp. 17 391–17 408.
- [54] M. Longland, D. Liebowitz, K. Moore, and S. S. Kanhere, "Text-conditioned graph generation using discrete graph variational autoencoders," 2022.
- [55] R. Lo, A. Datar, and A. Sridhar, "Lic-gan: Language information conditioned graph generative gan model," *arXiv preprint arXiv:2306.01937*, 2023.
- [56] J. Sohl-Dickstein, E. Weiss, N. Maheswaranathan, and S. Ganguli, "Deep unsupervised learning using nonequilibrium thermodynamics," in *International Conference on Machine Learning (ICML)*, 2015, pp. 2256–2265.
- [57] J. Ho, A. Jain, and P. Abbeel, "Denoising diffusion probabilistic models," *Advances in Neural Information Processing Systems (NeurIPS)*, vol. 33, pp. 6840–6851, 2020.
- [58] Y. Song, J. Sohl-Dickstein, D. P. Kingma, A. Kumar, S. Ermon, and B. Poole, "Score-based generative modeling through stochastic differential equations," in *International Conference on Learning Representations (ICLR)*, 2020.
- [59] E. Hoogeboom, D. Nielsen, P. Jaini, P. Forré, and M. Welling, "Argmax flows and multinomial diffusion: Learning categorical distributions," *Advances in Neural Information Processing Systems (NeurIPS)*, vol. 34, pp. 12 454–12 465, 2021.
- [60] J. Austin, D. D. Johnson, J. Ho, D. Tarlow, and R. Van Den Berg, "Structured denoising diffusion models in discrete state-spaces," *Advances in Neural Information Processing Systems (NeurIPS)*, vol. 34, pp. 17 981–17 993, 2021.
- [61] R. Zhang, P. Isola, and A. A. Efros, "Colorful image colorization," in *European Conference on Computer Vision (ECCV)*, 2016, pp. 649–666.
- [62] E. Jang, S. Gu, and B. Poole, "Categorical reparameterization with gumbel-softmax," in *International Conference on Learning Representations (ICLR)*, 2016.
- [63] A. Ramesh, M. Pavlov, G. Goh, S. Gray, C. Voss, A. Radford, M. Chen, and I. Sutskever, "Zero-shot

- text-to-image generation,” in *International Conference on Machine Learning (ICML)*, 2021, pp. 8821–8831.
- [64] S. Gu, D. Chen, J. Bao, F. Wen, B. Zhang, D. Chen, L. Yuan, and B. Guo, “Vector quantized diffusion model for text-to-image synthesis,” in *Proceedings of the IEEE/CVF Conference on Computer Vision and Pattern Recognition (CVPR)*, 2022, pp. 10 696–10 706.
- [65] Y. Zhou, C. Barnes, J. Lu, J. Yang, and H. Li, “On the continuity of rotation representations in neural networks,” in *Proceedings of the IEEE/CVF Conference on Computer Vision and Pattern Recognition (CVPR)*, 2019, pp. 5745–5753.
- [66] E. Perez, F. Strub, H. De Vries, V. Dumoulin, and A. Courville, “Film: Visual reasoning with a general conditioning layer,” in *Proceedings of the AAAI conference on Artificial Intelligence (AAAI)*, vol. 32, 2018.
- [67] V. P. Dwivedi and X. Bresson, “A generalization of transformer networks to graphs,” in *AAAI Workshop on Deep Learning on Graphs: Methods and Applications*, 2021.
- [68] J. L. Ba, J. R. Kiros, and G. E. Hinton, “Layer normalization,” *arXiv preprint arXiv:1607.06450*, 2016.
- [69] P. Dhariwal and A. Nichol, “Diffusion models beat gans on image synthesis,” *Advances in Neural Information Processing Systems (NeurIPS)*, vol. 34, pp. 8780–8794, 2021.
- [70] A. Radford, J. W. Kim, C. Hallacy, A. Ramesh, G. Goh, S. Agarwal, G. Sastry, A. Askell, P. Mishkin, J. Clark *et al.*, “Learning transferable visual models from natural language supervision,” in *International Conference on Machine Learning (ICML)*, 2021, pp. 8748–8763.
- [71] J. Lei, C. Deng, B. Shen, L. Guibas, and K. Daniilidis, “Nap: Neural 3d articulation prior,” in *Advances in Neural Information Processing Systems (NeurIPS)*, 2023.
- [72] H. Fu, B. Cai, L. Gao, L.-X. Zhang, J. Wang, C. Li, Q. Zeng, C. Sun, R. Jia, B. Zhao *et al.*, “3d-front: 3d furnished rooms with layouts and semantics,” in *Proceedings of the IEEE/CVF International Conference on Computer Vision (ICCV)*, 2021, pp. 10 933–10 942.
- [73] M. Heusel, H. Ramsauer, T. Unterthiner, B. Nessler, and S. Hochreiter, “Gans trained by a two time-scale update rule converge to a local nash equilibrium,” *Advances in Neural Information Processing Systems (NeurIPS)*, vol. 30, 2017.
- [74] T. Kynkäänniemi, T. Karras, M. Aittala, T. Aila, and J. Lehtinen, “The role of imagenet classes in fréchet inception distance,” in *International Conference on Learning Representations (ICLR)*, 2022.
- [75] M. Bińkowski, D. J. Sutherland, M. Arbel, and A. Gretton, “Demystifying mmd gans,” in *International Conference on Learning Representations (ICLR)*, 2018.
- [76] B. O. Community, *Blender - a 3D modelling and rendering package*, Blender Foundation, Stichting Blender Foundation, Amsterdam, 2018. [Online]. Available: <http://www.blender.org>
- [77] C. Meng, Y. He, Y. Song, J. Song, J. Wu, J.-Y. Zhu, and S. Ermon, “Sdedit: Guided image synthesis and editing with stochastic differential equations,” in *International Conference on Learning Representations (ICLR)*, 2021.
- [78] A. Q. Nichol, P. Dhariwal, A. Ramesh, P. Shyam, P. Mishkin, B. McGrew, I. Sutskever, and M. Chen, “Glide: Towards photorealistic image generation and editing with text-guided diffusion models,” in *International Conference on Machine Learning (ICML)*, 2022, pp. 16 784–16 804.
- [79] R. Suvorov, E. Logacheva, A. Mashikhin, A. Remizova, A. Ashukha, A. Silvestrov, N. Kong, H. Goka, K. Park, and V. Lempitsky, “Resolution-robust large mask inpainting with fourier convolutions,” in *Proceedings of the IEEE/CVF Winter Conference on Applications of Computer Vision (WACV)*, 2022, pp. 2149–2159.

APPENDIX A DATASET DETAILS

A.1 3D Indoor Scene-Instruction Paired Dataset

Following previous works [17; 20; 21], we use three types of indoor rooms in 3D-FRONT [72] and preprocess the dataset by filtering some problematic samples, resulting in 4041 bedrooms, 813 living rooms and 900 dining rooms. The number of objects N_i in the valid bedrooms is between 3 and 12 with 21 object categories, i.e., $K_c = 21$. While for living and dining rooms, N_i varies from 3 to 21 and $K_c = 24$. We use the same data split for training and evaluation as ATISS [17].

The original 3D-FRONT dataset does not contain any descriptions of room layout or object appearance details. To advance research in the field of text-conditional indoor scene generation, we carefully curate a high-quality dataset with paired scenes and instructions for interior design through a multi-step process:

- 1) **Spatial Relation Extraction:** View-dependent spatial relations are initially extracted from the 3D-FRONT dataset using predefined rules listed in Appendix A.3.
- 2) **Object Captioning:** We further enhance the dataset by providing captions to objects using BLIP [27], a powerful model pretrained for vision-language understanding, given furniture 2D thumbnail images from the original dataset [72].
- 3) **Caption Refinement:** As generated captions may not always be accurate, we filter them with corresponding ground-truth categories using ChatGPT [28; 29], a large language model fine-tuned for instruction-based tasks. This results in precise and expressive descriptions of each object in the scene. The prompt and hyperparameters for ChatGPT to filter captions are provided in Appendix A.4.
- 4) **Instruction Generation:** The final instructions for scene synthesis are derived from 1 \sim 2 randomly selected “(subject, relation, object)” triplets obtained during the first extraction process. Verbs and conjunctions within sentences are also randomly picked to maintain diversity and fluency.

A.2 2D E-commerce Poster-Instruction Paired Dataset

Several efforts have been made to create public datasets for 2D poster design, as shown in Table 7. CGL-GAN [41] and PosterLayout [10] provide large-scale poster datasets accompanied by bounding box annotations. CapOnImage2M [43] gathers product descriptions and annotated taglines for elements in posters, offering richer information for poster generation. AutoPoster [12] innovatively introduces a dataset featuring tagline and element attribute annotations. However, to the best of our knowledge, no existing dataset provides comprehensive information for instruction-driven poster synthesis.

In this work, we bridge this gap by constructing a high-quality E-commerce poster dataset based on AutoPoster [12]:

- 1) **Instruction Generation:** Firstly, we employ predefined rules as shown in Appendix A.3 to extract spatial relations between 2D objects based on the place of

their bounding boxes. With the annotation of graphic features, we can derive descriptions of objects in terms of colors, shapes, and fonts. Since the names of colors in LAB space can be ambiguous, we opt to use the nearest match in Web Standard Color palette as the name of each color. Then, we randomly choose several “(subject, relation, object)” triplets and pick up verbs and conjunctions to formulate an instruction.

- 2) **Product Descriptions:** We obtained product descriptions from the Internet by web crawler techniques and manually checked and filtered them, resulting in **73,070** pieces of product descriptions.
- 3) **Clean Product Images:** In accordance with the improved strategy outlined in Sec. 5.1 for inpainting final posters, we obtained clean product images of significantly higher quality compared to the previous method. The comparisons between previous works [10; 12] are demonstrated in Figure 5.

We provide an example in Figure 6 to showcase various elements contained in our curated poster dataset.

A.3 Relation Definitions

Assume X and Y span the ground or poster plane, and Z is the vertical axis for 3D scenes only. We use `Center` to represent the coordinates of a bounding box’s center. `Height` is the Z -axis size of a 3D bounding box. Relative orientation is computed as $\theta_{so} := \text{atan2}(Y_s - Y_o, X_s - X_o)$, where s and o respectively refer to “subject” and “object” in a relationship. $d(s, o)$ is the ground distance between s and o . $\text{Inside}(s, o)$ indicates whether the subject center is inside the ground bounding box of the object. We define 11 relationships in both 3D and 2D space as listed in Table 8 and Table 9, respectively.

A.4 Caption Refinement by ChatGPT

The generated 3D object captions from BLIP are refined by ChatGPT (`gpt-3.5-turbo`). Our prompt to ChatGPT is provided in Table 10. We set the hyperparameter `temperature` and `top_p` for text generation to 0.2 and 0.1 respectively, encouraging more deterministic and focused outputs.

APPENDIX B QUALITATIVE RESULTS

B.1 Instruction-driven 3D Scene Synthesis

We present visualizations of instruction-driven synthesized 3D scenes in Figure 7, 8 and 9. Besides the quantitative evaluations shown in Table 1, these qualitative visualizations also show the superiority of our method over previous state-of-the-art approaches in terms of adherence to instructions and generative quality.

B.2 Zero-shot 3D Scene Applications

We present visualizations illustrating various zero-shot instruction-driven applications, including stylization, rearrangement, completion, and unconditional 3D scene synthesis in Figure 10, 11, 12 and 13 respectively. We find that the autoregressive model ATISS [17] tends to generate

TABLE 7: Comparison of the types of elements contained in various poster datasets.

Dataset	Data Type	Instruction	Product Information		Graphic Element Annotation			Poster
			Image	Description	Category	Bounding Box	Attribute	
CGL-GAN [41]					✓	✓		✓
PosterLayout [10]			✓		✓	✓		✓
CapOnImage2M [43]				✓	✓	✓	✓	✓
AutoPoster[12]					✓	✓	✓	✓
Ours		✓	✓	✓	✓	✓	✓	✓

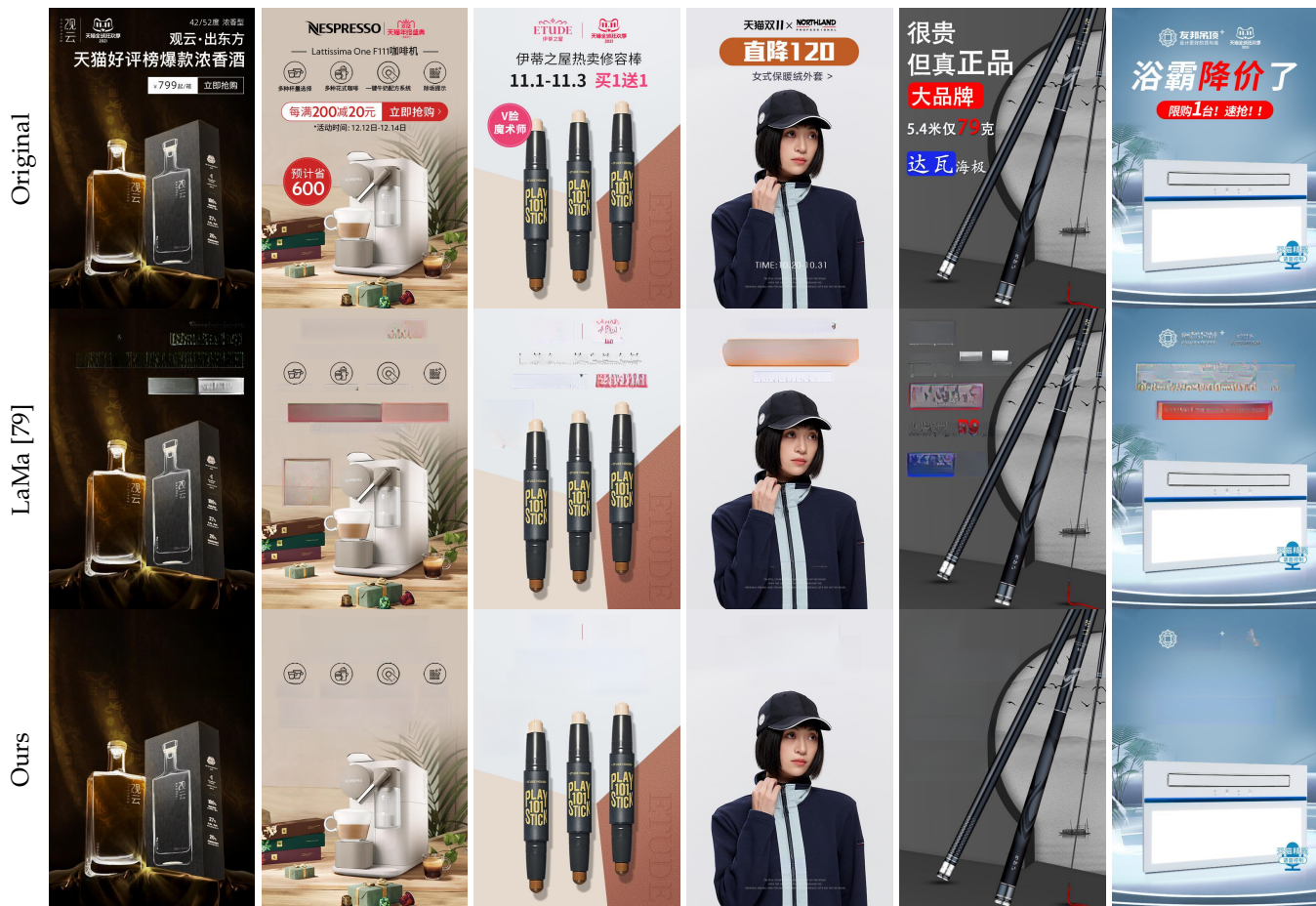


Fig. 5: Comparisons of inpainting results between our strategy and the original LaMa [79].

redundant objects, resulting in chaotic synthesized scenes. DiffuScene [21] encounters challenges in accurately modeling object semantic features, often yielding objects that lack coherence in terms of style or pairing, thereby diminishing the aesthetic appeal of the synthesized scenes. Moreover, both baseline models frequently struggle to follow the provided instructions during conditional generation.

B.3 Instruction-driven 2D Poster Synthesis

Comparisons of our synthesized 2D posters with other state-of-the-art methods are shown in Figure 14, 15, and 16, demonstrating the superiority of our method compared to previous state-of-the-art approaches in terms of better mimicking the behavior of human designers and following provided instructions.

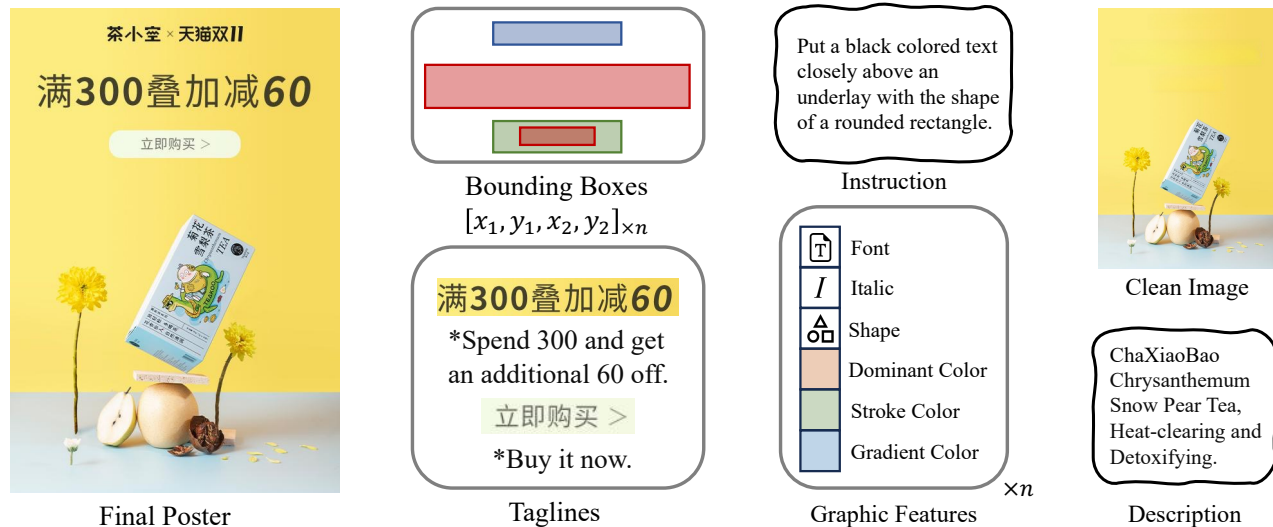


Fig. 6: An example from our comprehensive 2D E-commerce poster dataset.

TABLE 8: Rules to determine the spatial relationships between objects in a 3D scene.

Relationship	Rule
Left of	$(\theta_{so} \geq \frac{3\pi}{4} \text{ or } \theta_{so} < -\frac{3\pi}{4}) \text{ and } 1 < d(s, o) \leq 3$
Right of	$-\frac{\pi}{4} \leq \theta_{so} < \frac{\pi}{4} \text{ and } 1 < d(s, o) \leq 3$
In front of	$\frac{\pi}{4} \leq \theta_{so} < \frac{3\pi}{4} \text{ and } 1 < d(s, o) \leq 3$
Behind	$-\frac{3\pi}{4} \leq \theta_{so} < -\frac{\pi}{4} \text{ and } 1 < d(s, o) \leq 3$
Closely left of	$(\theta_{so} \geq \frac{3\pi}{4} \text{ or } \theta_{so} < -\frac{3\pi}{4}) \text{ and } d(s, o) \leq 1$
Closely right of	$-\frac{\pi}{4} \leq \theta_{so} < \frac{\pi}{4} \text{ and } d(s, o) \leq 1$
Closely in front of	$\frac{\pi}{4} \leq \theta_{so} < \frac{3\pi}{4} \text{ and } d(s, o) \leq 1$
Closely behind	$-\frac{3\pi}{4} \leq \theta_{so} < -\frac{\pi}{4} \text{ and } d(s, o) \leq 1$
Above	$(\text{Center}_{Z_s} - \text{Center}_{Z_o}) > (\text{Height}_s + \text{Height}_o)/2$ and $(\text{Inside}(s, o) \text{ or } \text{Inside}(o, s))$
Below	$(\text{Center}_{Z_o} - \text{Center}_{Z_s}) > (\text{Height}_s + \text{Height}_o)/2$ and $(\text{Inside}(s, o) \text{ or } \text{Inside}(o, s))$
None	$d(s, o) > 3$

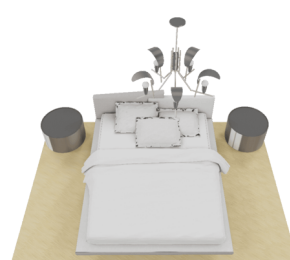
TABLE 9: Rules to determine the spatial relationships between objects in a 2D poster.

Relationship	Rule
Left of	$(\theta_{so} \geq \frac{3\pi}{4} \text{ or } \theta_{so} < -\frac{3\pi}{4}) \text{ and } 80 < d(s, o) \leq 300$
Right of	$-\frac{\pi}{4} \leq \theta_{so} < \frac{\pi}{4} \text{ and } 80 < d(s, o) \leq 300$
above	$\frac{\pi}{4} \leq \theta_{so} < \frac{3\pi}{4} \text{ and } 80 < d(s, o) \leq 300$
below	$-\frac{3\pi}{4} \leq \theta_{so} < -\frac{\pi}{4} \text{ and } 80 < d(s, o) \leq 300$
Closely left of	$(\theta_{so} \geq \frac{3\pi}{4} \text{ or } \theta_{so} < -\frac{3\pi}{4}) \text{ and } d(s, o) \leq 80$
Closely right of	$-\frac{\pi}{4} \leq \theta_{so} < \frac{\pi}{4} \text{ and } d(s, o) \leq 80$
Closely above	$\frac{\pi}{4} \leq \theta_{so} < \frac{3\pi}{4} \text{ and } d(s, o) \leq 80$
Closely below	$-\frac{3\pi}{4} \leq \theta_{so} < -\frac{\pi}{4} \text{ and } d(s, o) \leq 80$
Enclosing	$\text{Inside}(o, s)$
Enclosed with	$\text{Inside}(s, o)$
None	$d(s, o) > 300$

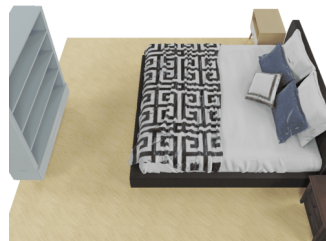
TABLE 10: Prompt for ChatGPT to refine raw 3D object descriptions.

Given a description of furniture from a captioning model and its ground-truth category, please combine their information and generate a new short description in one line. The provided category must be the descriptive subject of the new description. The new description should be as short and concise as possible, encoded in ASCII. Do not describe the background and counting numbers. Do not describe size like 'small', 'large', etc. Do not include descriptions like 'a 3D model', 'a 3D image', 'a 3D printed', etc. Descriptions such as color, shape and material are very important, you should include them. If the old description is already good enough, you can just copy it. If the old description is meaningless, you can just only include the category. For example: Given 'a 3D image of a brown sofa with four wooden legs' and 'multi-seat sofa', you should return: a brown multi-seat sofa with wooden legs. Given 'a pendant lamp with six hanging balls on the white background' and 'pendant lamp', you should return: a pendant lamp with hanging balls. Given 'a black and brown chair with a floral pattern' and 'armchair', you should return: a black and brown floral armchair. The above examples indicate that you should delete the redundant words in the old description, such as '3D image', 'four', 'six' and 'white background', and you must include the category name as the subject in the new description. The old descriptions is '{BLIP caption}', its category is '{ground-truth category}', the new descriptions should be:

Add a corner side table with a round top to the left of a black and silver pendant lamp with lights.



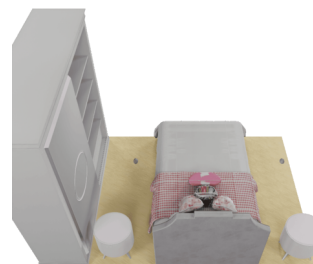
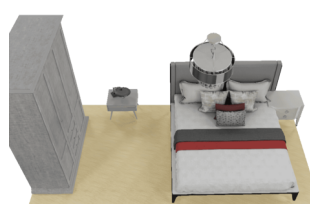
Add a grey stool with black legs behind a wooden bookshelf with shelves. Set up a bookshelf left of a black and white double bed.



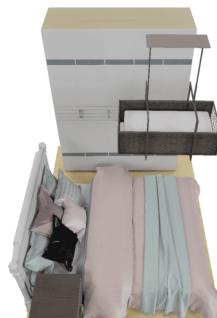
Add a black and grey double bed in front of a black wardrobe with hanging clothes. Add a black pendant lamp with a handle in front of a wardrobe.



Add a double bed left of a gray nightstand with drawers. Place a gray nightstand with drawers to the right of a gray wardrobe with shelves and drawers.



Add a wooden wardrobe with drawers behind a brown and black double bed. Additionally, install a pendant lamp in front of a wooden wardrobe with drawers.



(a) Instructions

(b) ATISS

(c) DiffuScene

(d) Ours

Fig. 7: Visualizations for instruction-drive synthesized 3D bedrooms by ATISS [17], DiffuScene [21] and our method.

Place a dining table to the right of a coffee table. Put a black dining chair with a black frame right of a coffee table.



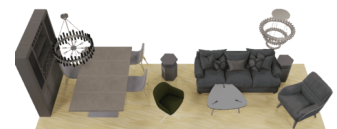
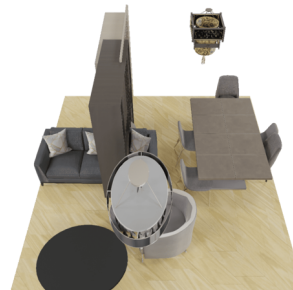
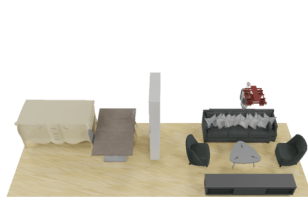
Set up a floral multi-seat sofa left of a coffee table.



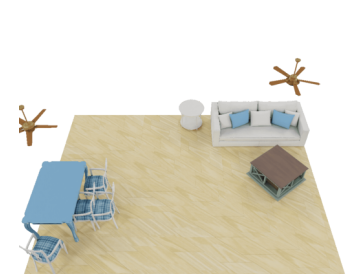
Put a pendant lamp with white shades above a wooden coffee table with carved legs.



Set up a brown dining table with metal legs left of a lounge chair. Then, set up a red pendant lamp with a handle behind a black bookshelf with shelves and a drawer.



Add a blue dining table with a wooden top behind a blue plaid upholstered dining chair. Place a metal corner side table to the left of a blue multi-seat sofa.



(a) Instructions

(b) ATISS

(c) DiffuScene

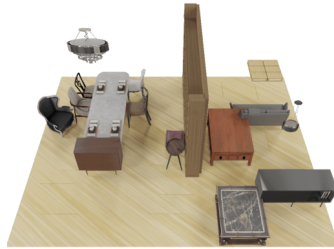
(d) Ours

Fig. 8: Visualizations for instruction-drive synthesized 3D living rooms by ATISS [17], DiffuScene [21] and our method.

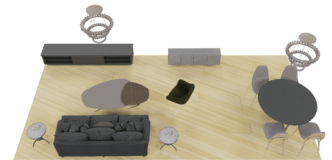
Place a dining chair *closely in front of* a dining table. Put a dining table *below* a pendant lamp.



Place a burgundy dining chair to the *close right of* a dining table.



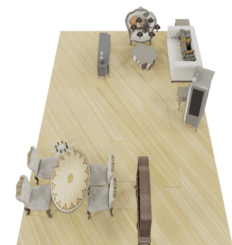
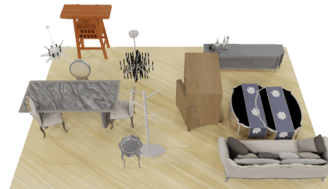
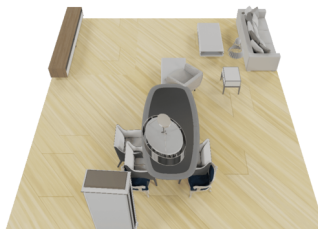
Position a brown dining table with metal legs *closely behind* a grey fabric dining chair. Additionally, arrange a triangle coffee table to the *left of* a black multi-seat sofa with pillows.



Set up a dining table *closely right of* a wooden dining chair.



Place a dining table *in front of* a silver wine cabinet with a black door. Then, arrange a metal pendant lamp with a hanging rod to the *left of* a multi-seat sofa.



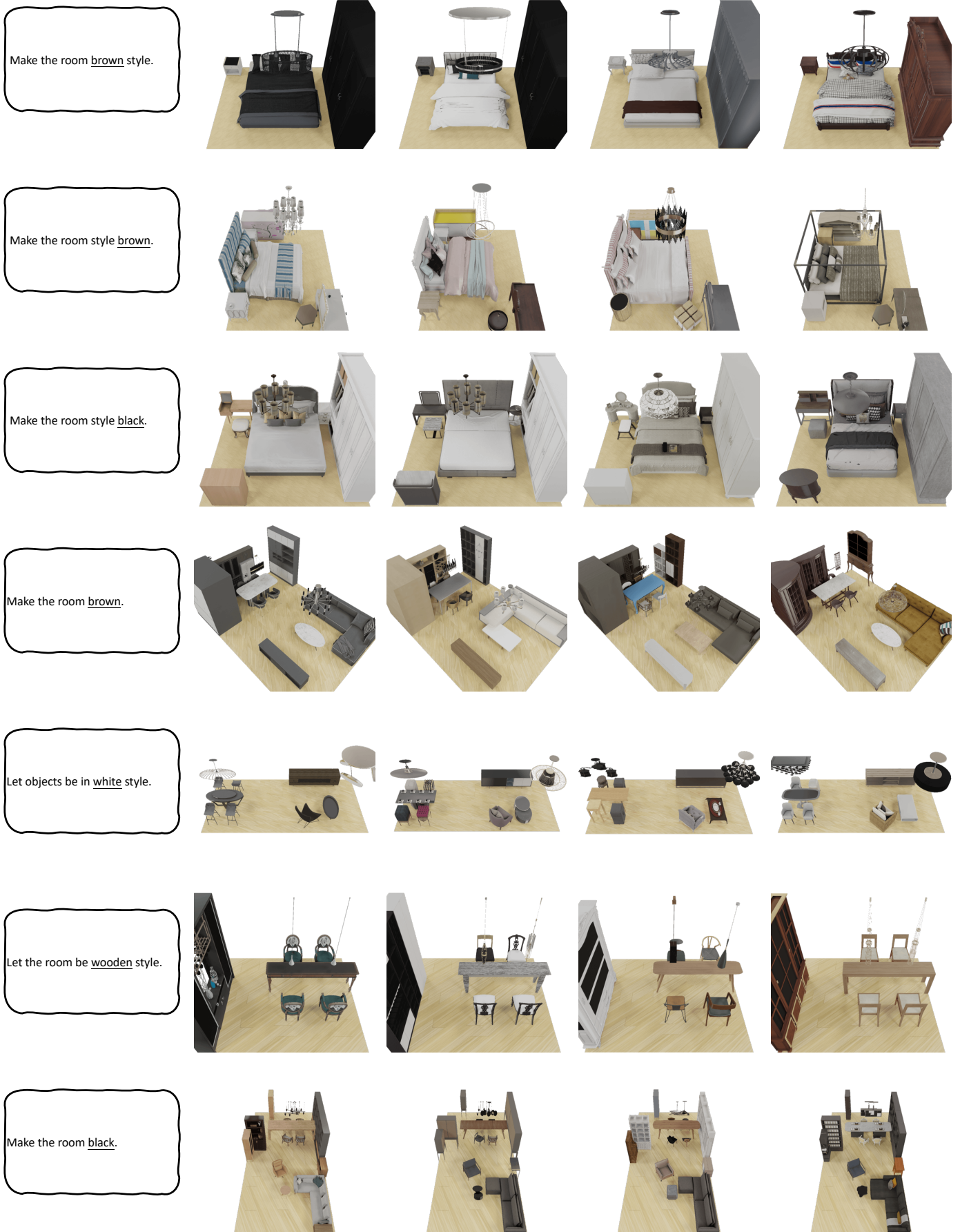
(a) Instructions

(b) ATISS

(c) DiffuScene

(d) Ours

Fig. 9: Visualizations for instruction-drive synthesized 3D dining rooms by ATISS [17], DiffuScene [21] and our method.



(a) Instructions

(b) Original Scenes

(c) ATISS

(d) DiffuScene

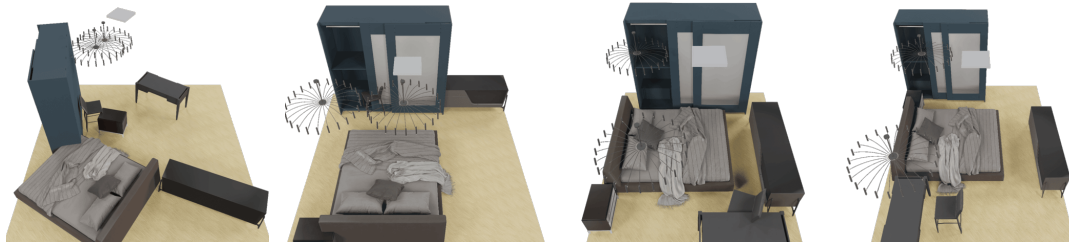
(e) Ours

Fig. 10: Visualizations for instruction-drive 3D scenes stylization by ATISS [17], DiffuScene [21] and our method.

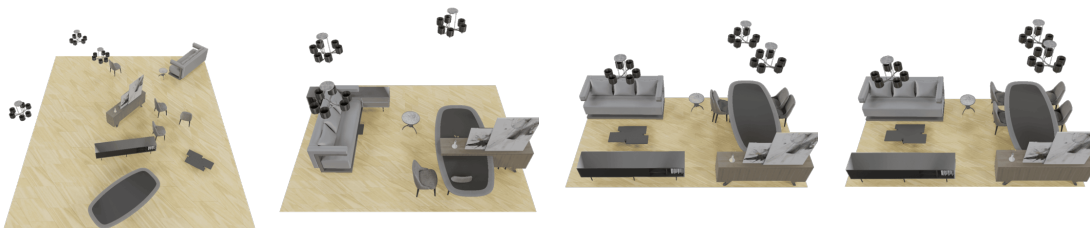
Place a blue wardrobe *left of* a blue double bed.



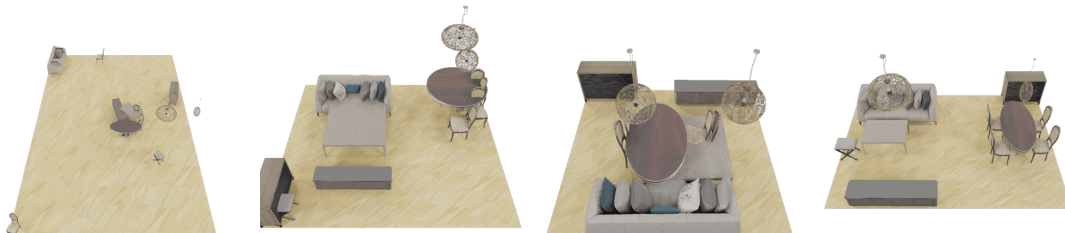
Put a black desk with drawers in front of a double bed.



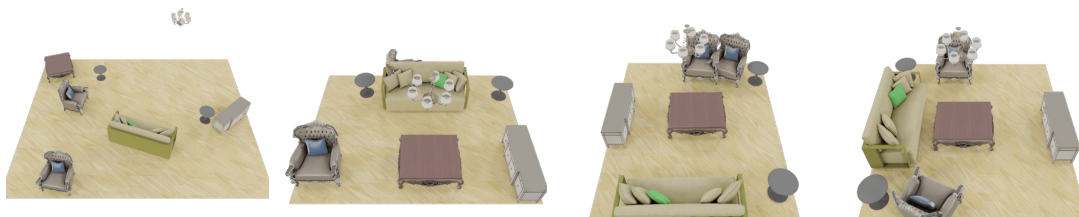
Set up a grey multi-seat sofa with pillows *behind* a black pendant lamp with six pots. Next, arrange a grey dining chair to the *right of* a multi-seat sofa.



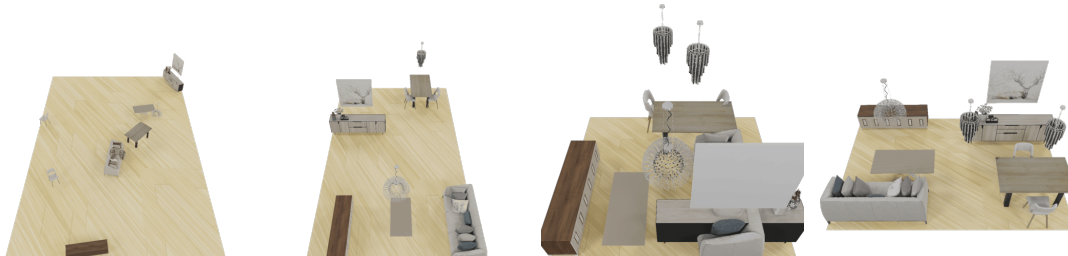
Position a patterned dining chair *right of* a multi-seat sofa with pillows. Additionally, put a black TV stand in front of a multi-seat sofa with pillows.



Put a green multi-seat sofa to the *left of* a wooden coffee table with carved legs. And put an armchair *behind* a wooden coffee table with carved legs.



Position a multi-seat sofa *left of* a dining table with a wooden top. Then, arrange a modern pendant lamp with a metal ball *in front of* a brown and grey TV stand.



Arrange a white dining table to the *right of* a black console table.



(a) Instructions

(b) Messy Scenes

(c) ATISS

(d) DiffuScene

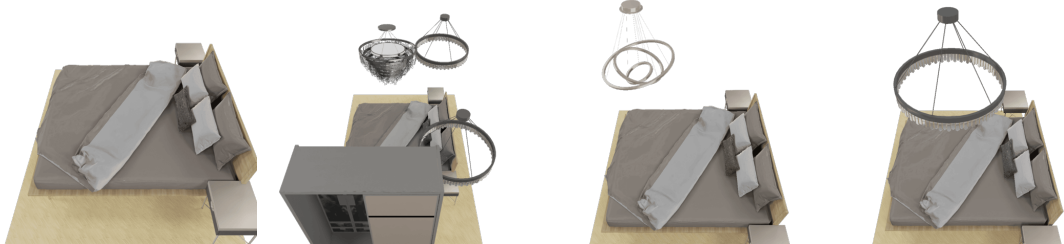
(e) Ours

Fig. 11: Visualizations for instruction-drive 3D scenes re-arrangement by ATISS [17], DiffuScene [21] and our method.

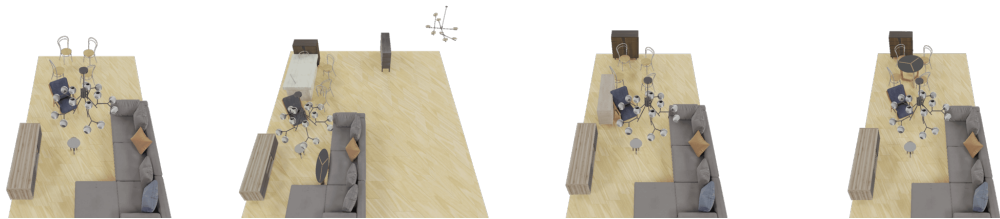
Add a wooden wardrobe with drawers *behind* a brown and black double bed. Additionally, install a pendant lamp *in front* of a wooden wardrobe with drawers.



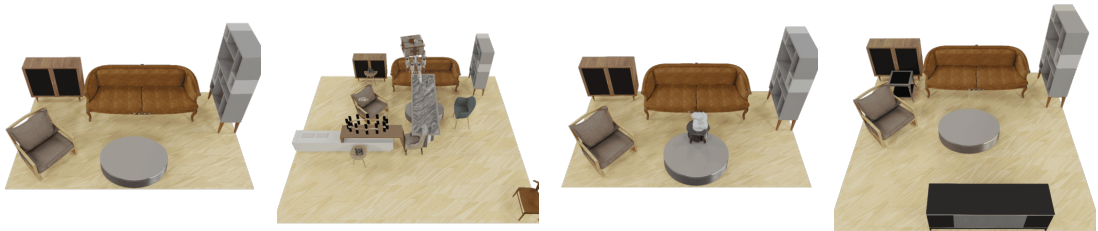
Position a black and white circular pendant lamp *behind* a black and silver nightstand with a drawer.



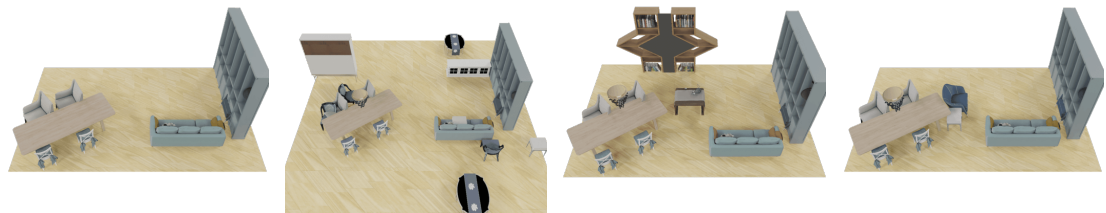
Place a wardrobe *behind* a wooden dining chair.



Set up a TV stand *in front* of a brown loveseat sofa with a wooden frame.



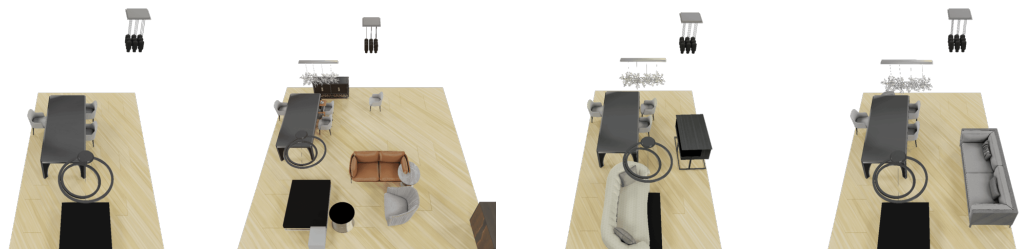
Position a blue armchair *left* of a multi-seat sofa. Then, Put a silver coffee table *left* of a multi-seat sofa.



Put a wooden dining table *below* a pendent lamp.



Put a black multi-seat sofa with pillows to the *right* of a black plastic dining table.



(a) Instructions

(b) Partial Scenes

(c) ATISS

(d) DiffuScene

(e) Ours

Fig. 12: Visualizations for instruction-drive 3D scenes completion by ATISS [17], DiffuScene [21] and our method.

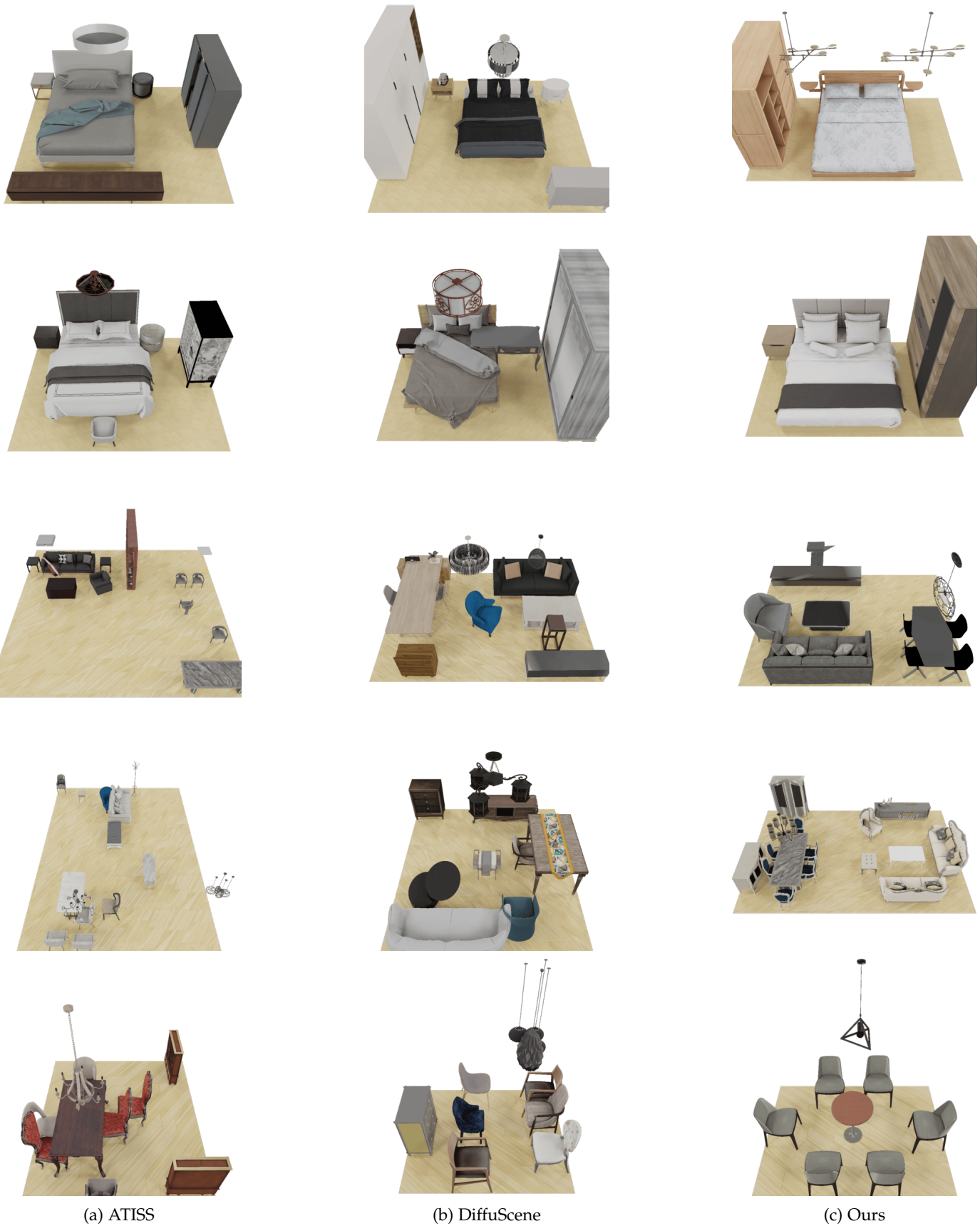


Fig. 13: Visualizations for unconditional 3D scenes stylization by ATISS [17], DiffuScene [21] and our method.



Fig. 14: Visualizations for instruction-drive synthesized 2D posters by LayoutTrans [6], LayoutVAE [7], LayoutDM [19] and our method. Note that posters are rendered according to synthesized graphic and textual features.

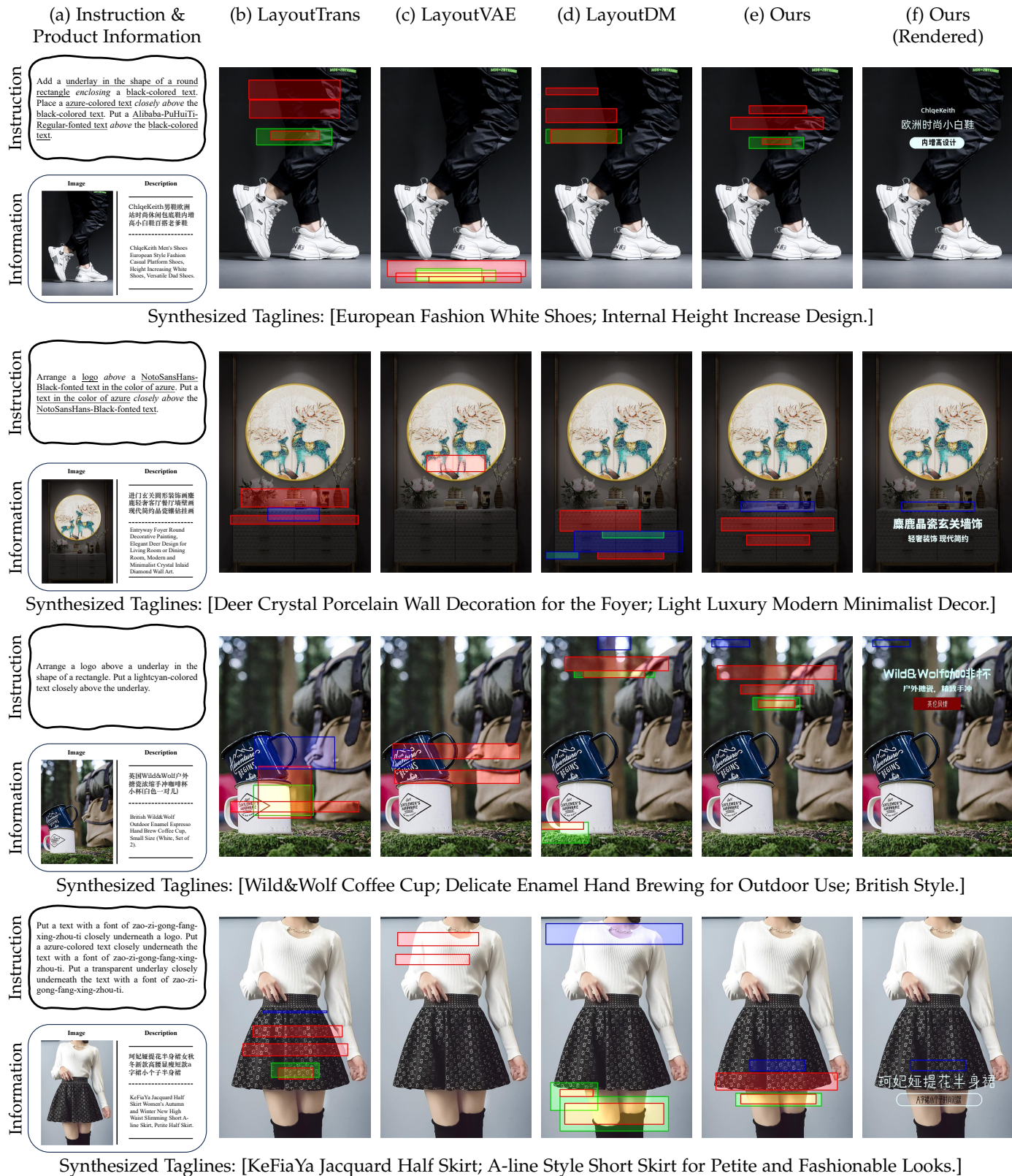


Fig. 15: Visualizations for instruction-drive synthesized 2D posters by LayoutTrans [6], LayoutVAE [7], LayoutDM [19] and our method. Note that posters are rendered according to synthesized graphic and textual features.

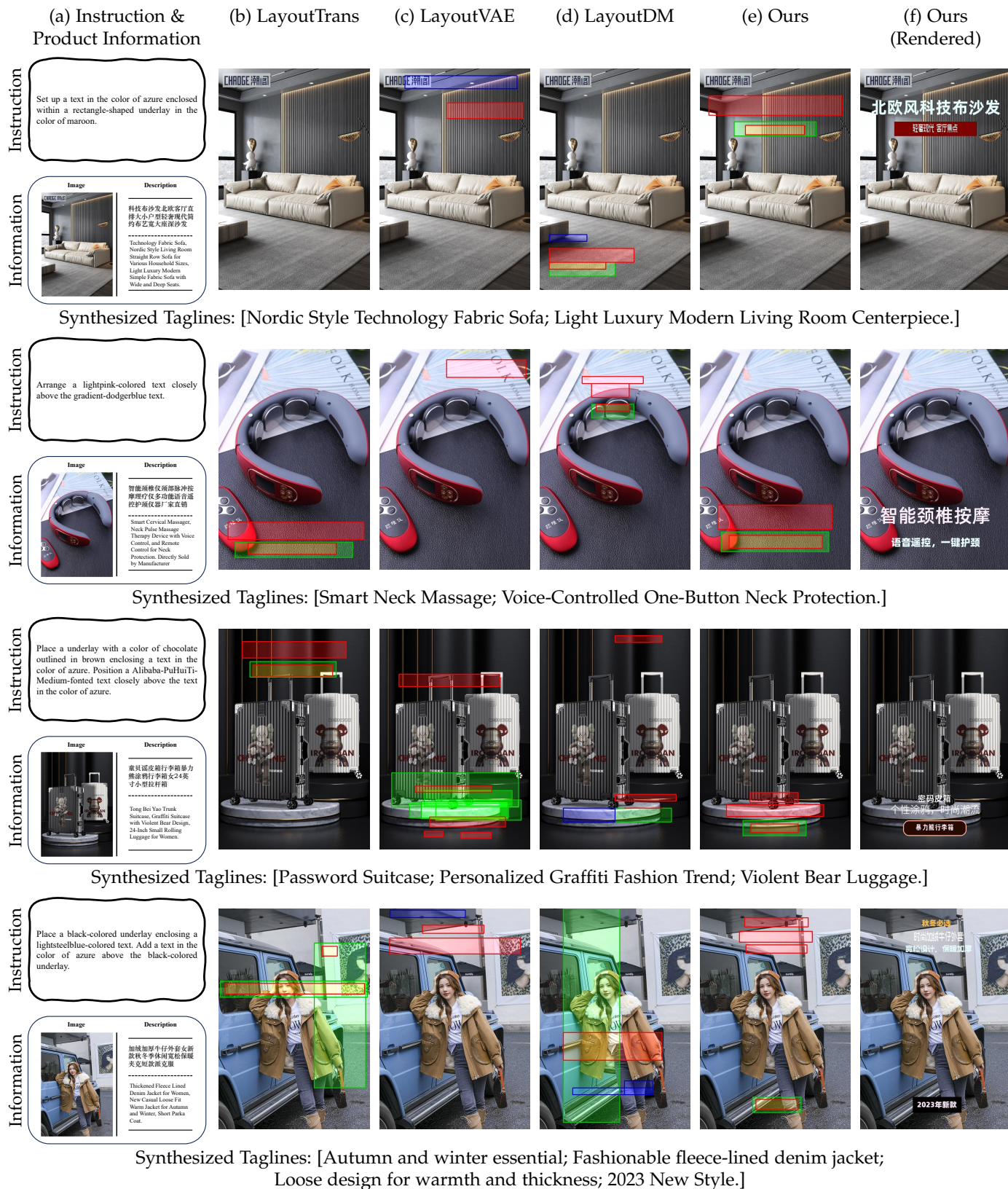


Fig. 16: Visualizations for instruction-drive synthesized 2D posters by LayoutTrans [6], LayoutVAE [7], LayoutDM [19] and our method. Note that posters are rendered according to synthesized graphic and textual features.